AD_____

Award Number: W81XWH-09-1-0658

TITLE: New Advanced Technologies in Stem Cell Therapy

PRINCIPAL INVESTIGATOR: Dr. Johnny Huard

CONTRACTING ORGANIZATION: The University of Pittsburgh
Pittsburgh, PA 15213

REPORT DATE: September 2011

TYPE OF REPORT: Annual

PREPARED FOR: U.S. Army Medical Research and Materiel Command
Fort Detrick, Maryland 21702-5012

DISTRIBUTION STATEMENT: Approved for public release; distribution unlimited

REPORT DOCUMENTATION PAGE

Form Approved
OMB No. 0704-0188

1. REPORT DATE *(DD-MM-YYYY)*	**2. REPORT TYPE**	**3. DATES COVERED** *(From - To)*
01-09-2011	Annual	1 SEP 2010 - 31 AUG 2011

4. TITLE AND SUBTITLE

New Advanced Technologies in Stem Cell Therapy

5a. CONTRACT NUMBER

5b. GRANT NUMBER

W81XWH-09-1-0658

5c. PROGRAM ELEMENT NUMBER

6. AUTHOR(S)

Dr. Johnny Huard

E-Mail: jhuard@pitt.edu

5d. PROJECT NUMBER

5e. TASK NUMBER

5f. WORK UNIT NUMBER

7. PERFORMING ORGANIZATION NAME(S) AND ADDRESS(ES)

The University of Pittsburgh

Pittsburgh, PA 15213

8. PERFORMING ORGANIZATION REPORT NUMBER

9. SPONSORING / MONITORING AGENCY NAME(S) AND ADDRESS(ES)

U.S. Army Medical Research and Materiel Command
Fort Detrick, Maryland 21702-5012

10. SPONSOR/MONITOR'S ACRONYM(S)

11. SPONSOR/MONITOR'S REPORT NUMBER(S)

12. DISTRIBUTION / AVAILABILITY STATEMENT

Approved for Public Release; Distribution Unlimited

13. SUPPLEMENTARY NOTES

14. ABSTRACT

Abstract on next page

15. SUBJECT TERMS

Project 1: Duchenne Muscular Dystrophy (DMD), human muscle-derived cells (hMDC), myoendothelial cells, pericytes, hMDC transplantation, angiogenesis Project 2: Hepatacyte transplantation, inducible pluripotent stem (iPS)cells, alpha-1-antitrypsin (AT) deficiency, PiZ mice

16. SECURITY CLASSIFICATION OF:			**17. LIMITATION OF ABSTRACT**	**18. NUMBER OF PAGES**	**19a. NAME OF RESPONSIBLE PERSON**
a. REPORT	**b. ABSTRACT**	**c. THIS PAGE**			USAMRMC
U	U	U	UU	52	**19b. TELEPHONE NUMBER** *(include area code)*

Abstracts

Project 1

Background: We have isolated and characterized a population of skeletal muscle-derived stem cells (MDSCs) that display a greatly improved skeletal and cardiac muscle transplantation capacity when compared to skeletal muscle myoblasts. The MDSCs' ability to withstand oxidative and inflammatory stresses appears to be the single most important factor for their improved transplantation capacity. Although the true origin of MDSCs remains unclear, their high degree of similarity with blood vessel-derived stem cells suggests their potential origin could be from the vascular wall. We have recently isolated two distinct populations of cells from the vasculature of human skeletal muscle known collectively as human skeletal muscle-derived cells (hMDCs). The two populations are myo-endothelial cells and pericytes and both can repair skeletal and cardiac muscles in a more effective manner than myoblasts, as is observed with murine MDSCs.

In the current proposal we intend to evaluate and compare the regeneration capacity of these two hMDC populations after their implantation into the skeletal muscle of immunodeficient/dystrophic (SCID/mdx) mice. We will then investigate the influence that sex has on the regeneration and repair capacity of the hMDCs endowed with the greatest regeneration capacity (either myo-entothelial cells or pericytes). Finally we will investigate the influence that age plays on the regeneration capacity of the cells.

Study Design: We will investigate the effects of cell survival, proliferation, resistance to stress, and neo-angiogenesis on the regeneration capacity of the hMDCs implanted into the skeletal muscle of SCID/mdx mice Since we have observed that female murine MDSCs display an improved transplantation capacity in skeletal muscle when compared to male MDSCs, we will determine the influence that sex has on the hMDCs. Due to the fact that MDSCs isolated from aged mice have a lower skeletal muscle regeneration index than MDSCs isolated from young mice, we will also investigate the influence that donor and host age has on the isolated hMDCs.

Relevance: This project will enable us to further assess the feasibility of using hMDC transplantation to improve the function of skeletal muscle that has been damaged by Duchenne muscular dystrophy (DMD) and other muscle degenerative disorders and injury.

Technical Objective #1: To compare the regeneration capacities of human muscle-derived myo-endo cells and pericytes when implanted in the skeletal muscle of *SCID/mdx* mice and select the optimal cell type to proceed with Technical Objectives 2 and 3.

Hypothesis 1: A differential regeneration capacity will be observed in skeletal muscle of SCID/mdx mice between myo-endo cells and pericytes.

Technical Objective #2: To investigate the influence of sex on the regeneration/repair capacity of the hMDCs implanted in the skeletal muscle of *SCID/mdx* mice.

Hypothesis 2: After implantation into skeletal muscle, the hMDCs cells (myo-endo cells or pericytes) endowed with the highest regenerating potential in skeletal muscle will be influenced by the sex of the donor, due to a differential ability to resist stressful conditions.

Technical Objective #3: To investigate the influence of age on the regeneration/repair capacity of hMDCs implanted in the skeletal muscle of *SCID/mdx* mice.

Hypothesis 3: After implantation into skeletal muscle, the hMDCs cells (myo-endo cells or pericytes) endowed with the highest regenerating potential in skeletal muscle will be influenced by the age of the donor due to a differential ability to induce angiogenesis.

Project 2

Background: Hepatocyte transplantation holds great promise as an alternative to whole organ liver transplantation. Unfortunately, the availability of human hepatocytes is limited. We have shown that functionally normal hepatocytes can be generated from human ES cells (hES). Since human skin fibroblasts can now be genetically modified to produce (iPS) cells with characteristics nearly identical to hES cells, it may be possible to generate hepatocytes from patients using their own cells. We believe the PiZ transgenic mouse model of alpha-1-antitrypsin (AT) deficiency is critical for evaluating the efficacy of stem cell therapies, as hepatocytes without the mutant protein have a selective hepatic repopulation advantage in these mice, and the

PiZ mouse recapitulates the slowly progressing type of disease that affects most patients with chronic liver diseases.

Objective/Hypothesis: Both of the main obstacles to transplantation of stem cells for the treatment of liver disease (the number of livers available and the immunological barrier) might be addressed if liver cells could be generated de novo from precursor cells of the individual to be treated.

Study Design: We will determine the extent to which human patient-specific, inducible pluripotent stem (iPS) cells can be differentiated into primary human hepatocytes. We will then determine the extent to which the PiZ mouse model of AT deficiency can be developed as a platform for pre-clinical testing of hepatic stem cells. Finally, we will identify specific molecules responsible for regenerative and fibrotic signals in the PiZ mouse model of liver disease.

Relevance: This project will determine the extent to which patient-specific hepatic stem cells can be used for regeneration and repair of injuries to the liver and liver failure. A more complete understanding of the mechanisms by which donor stem cells can reduce liver injury and toxin and/or cancer risk should enhance the number of areas where hepatic stem cell transplantation might be effectively applied.

Technical Objective #1: *Determine the extent to which human patient-specific, inducible pluripotent stem (iPS) cells can be differentiated into primary human hepatocytes.*

Hypothesis: Protocols that successfully differentiate mouse and human embryonic stem (ES) cells toward a hepatocyte phenotype will be effective in differentiating human skin cell-derived iPS cells into liver cells.

Technical Objective #2: Determine the extent to which the PiZ mouse model of alpha-1-antitrypsin (AT) deficiency can be developed as a platform for pre-clinical testing of hepatic stem cell transplantation as a treatment for severe liver injury and disease.

Hypothesis: *iPS cells differentiated toward a hepatocyte phenotype can engraft and respond normally to proliferative signals in the livers of PiZ mice.*

Technical Objective #3: Utilize laser-capture microdissection, coupled with high-density oligonucleotide array techniques as well as double-label immunofluorescence techniques to identify specific molecules responsible for regenerative and fibrotic signals in the PiZ mouse model of liver disease.

Hypothesis: *Transplantation of donor stem cells can ameliorate liver injury and cancer risk in liver disease.*

Table of Contents

Sub-Project 1: Muscle stem cell transplantation for Duchenne muscular dystrophy
PI: Johnny Huard

INTRODUCTION:

We have isolated and characterized a population of skeletal muscle-derived stem cells (MDSCs) that display a greatly improved skeletal and cardiac muscle transplantation capacity when compared to skeletal muscle myoblasts. The MDSCs' ability to withstand oxidative and inflammatory stresses appears to be the single most important factor for their improved transplantation capacity. Although the true origin of MDSCs remains unclear, their high degree of similarity with blood vessel-derived stem cells suggests their potential origin could be from the vascular wall. We have also isolated two distinct populations of cells from the vasculature of human skeletal muscle known collectively as human skeletal muscle-derived cells (hMDCs). The two populations are myoendothelial cells and pericytes and they both can repair skeletal and cardiac muscles in a more effective manner than myoblasts, as is observed with murine MDSCs. In the current proposal we have evaluated and compared the regeneration capacity of these two hMDC populations in vitro and after their implantation into the skeletal muscle of immunodeficient/dystrophic (SCID/*mdx)* mice. We are now in the process of investigating the influence that sex has on the regeneration and repair capacity of the hMDCs endowed with the greatest regeneration capacity which we have determined to be the myoentothelial cell population. Finally we will investigate the influence that age plays on the regeneration capacity of the cells. We will investigate the effects of cell survival, proliferation, resistance to stress, and neo-angiogenesis on the regeneration capacity of the hMDCs implanted into the skeletal muscle of SCID/*mdx* mice Since we have observed that female murine MDSCs display an improved transplantation capacity in skeletal muscle when compared to male MDSCs, we will determine the influence that sex has on the hMDCs. Due to the fact that MDSCs isolated from aged mice have a lower skeletal muscle regeneration index than MDSCs isolated from young mice, we will also investigate the influence that donor and host age has on the isolated hMDCs. This project will enable us to further assess the feasibility of using hMDC transplantation to improve the function of skeletal muscle that has been damaged by Duchenne muscular dystrophy (DMD) and other muscle degenerative disorders and injury.

Last year we reported our group's progress in isolating and characterizing two population of hMDCs, myoendothelial cells and pericytes. Previous work with these two populations showed that the myoendothelial cells and pericytes could repair skeletal and cardiac muscle more effectively than myoblasts. As reported a year ago, several aspects of the first aim of the project were completed, namely the fluorescent-activated cell sorting (FACS) of the myoendothelial cells, pericytes and myoblasts from cryopreserved human progenitor skeletal muscle cells (hPSMCs); comparisons of the *in vitro* myogenic potential of these populations; and the transplantation of the populations into the cardiotoxin-injured skeletal muscle of SCID mice to assess their *in vivo* regenerative capacity. The results showed that the myoendothelial cells possessed a better in vitro myogenic differentiation capacity, as well as, a better in vivo engraftment capacity when transplanted into cardiotoxin injured skeletal muscle. Based on these data our team has spent the following year studying age and sex differences in the human myoendothelial cell populations.

BODY:

As outlined in our Statement of Work, this Progress Report for "**Sub-Project 1:** Muscle stem cell transplantation for Duchenne muscular dystrophy" will describe our current results related to Technical Objective 1 which is to be completed in Years 1 and 2.

Statement of Work:

Technical Objective #1: To compare the regeneration capacities of human muscle-derived myoendothelial cells and pericytes when implanted in the skeletal muscle of *SCID/mdx* mice and select the optimal cell type to proceed with Technical Objectives 2 and 3.

Hypothesis 1: A differential regeneration capacity will be observed in the skeletal muscle of SCID/mdx mice between myoendothelial cells and pericytes.

Technical Objective #2: To investigate the influence of sex on the regeneration/repair capacity of the hMDCs implanted in the skeletal muscle of *SCID/mdx* mice.

Hypothesis 2: After implantation into skeletal muscle, the hMDCs cells endowed with the highest regenerating potential in skeletal muscle will be influenced by the sex of the donor, due to a differential ability to resist stressful conditions.

Technical Objective #3: To investigate the influence of age on the regeneration/repair capacity of hMDCs implanted in the skeletal muscle of *SCID/mdx* mice.

Hypothesis 3: After implantation into skeletal muscle, the hMDCs cells endowed with the highest regenerating potential in skeletal muscle will be influenced by the age of the donor due to a differential ability to induce angiogenesis.

Technical Objective 1 will be performed during the first 2 years of funding. Years 3 and 4 will be devoted to completing **Technical Objectives 2 and 3**. **Objectives 2 and 3** can be performed simultaneously once we have determined the optimal cell type (myo-endo cells vs. pericyctes) as is outlined in **Technical Objective 1**.

Progress made from 9-1-10 to 8-31-11

Myogenic and proliferation capacity of young vs. old myoendothelial cells

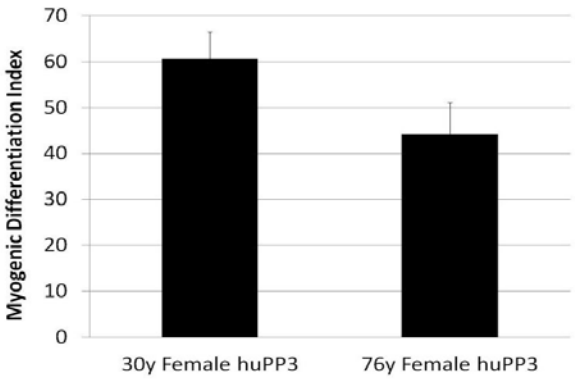

Figure 1: The MDI of two populations of human female myoendothelial cells. The MDI shows the cells isolated from the 30 year old female donor have a greater myogenic capacity than cells isolated from the 76 year old donor ($p < 0.05$).

In vitro assays to look at differences in myogenic capacities of young and old human myoendothelial cells were conducted using two cell populations one from a 30 year old female and the other from a 76 year old female. Both cell populations were derived from human skeletal muscle and isolated using our lab's pre-plate technique for stem cell isolation. Cells isolated from the latest preplate, preplate 3(PP3), were utilized in the current experiments (which means that the isolated cells adhered to the collagenated flasks between 24-48 hours after the initial muscle biopsy isolation and dissociation. For murine cell isolations, PP6 cells are able to be isolated and possess the highest multipotency and engraftment capacities as compared to PP1-PP5. To compare the myogenic capacities of the young and old cells in vitro, the cells were promoted to differentiate by placing them in low (2%) serum media for five days after which the cells were fixed and then stained for their expression of myosin heavy chain (MHC) and DAPI. The myogenic differentiation index (MDI) for each cell type was calculated by counting the number of nuclei inside MHC-stained differentiated myotubes and dividing this number by the total number of nuclei. The results shown in figure 1 indicated that the older female PP3 cells had a reduction in their myogenic potential (myotube formation) *in vitro* compared the cells isolated from the younger female biopsy. These results are being confirmed and the experiment is being repeated with human male myoendothelial cells, as well.

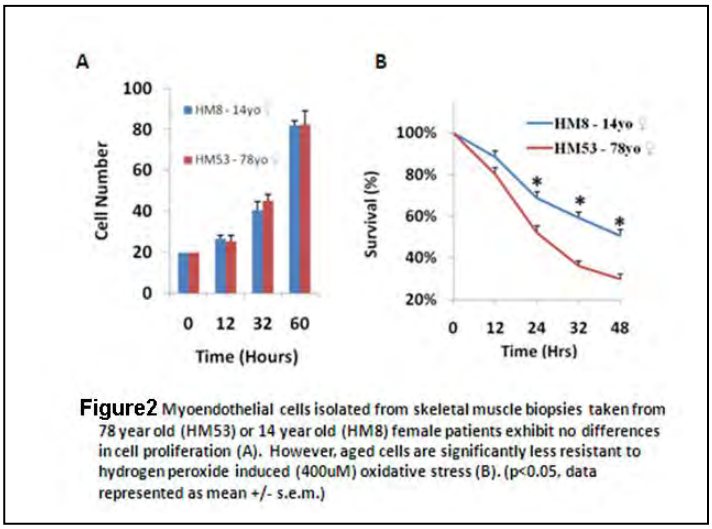

Figure2 Myoendothelial cells isolated from skeletal muscle biopsies taken from 78 year old (HM53) or 14 year old (HM8) female patients exhibit no differences in cell proliferation (A). However, aged cells are significantly less resistant to hydrogen peroxide induced (400uM) oxidative stress (B). ($p<0.05$, data represented as mean +/- s.e.m.)

In another set of experiments we isolated myoendothelial cells via FACS from the skeletal muscle of a 76 year old female (HM53) and a 14 year old female (HM8) patient. The cells were studied for their proliferative and oxidative stress resistance (exposure to 400uM hydrogen peroxide) capacities. In this study the cells were found to not differ in their

proliferative capacity between HM53 and HM8 (Figure 2A); however there was a significant difference in their resistance to oxidative stress capacities at 24, 32 and 48 hrs post-exposure (Figure 2B, older cells displaying a reduction to stress resistance).

Additional studies are currently underway to increase the number of populations of young and old myoendothelial and PP3 cells (and sex) studied for their proliferation, myogenic and their stress resistance capacities.

Optimizing the culture conditions for expanding myoendothelial cells

It is of critical importance that the myoendothelial cells isolated from human skeletal muscle can be maintained in a "stem" like state when expanded in a cell monolayer. A media formulation of 10% fetal bovine serum, 10% horse serum, 1% penicillin/streptomycin and 1% chick embryo extract is normally used to culture the cells. This proliferation media (PRO) was combined with Endothelial Growth Media-2 (EGM2) media (Lonza) at a 1:1 mixture and designated PROe media. A 69 year old, male population of human myoendothelial cells (ST2) isolated via FACS were seeded on a 24-well plate at a density of 2000 cells/cm^2 of growth area. The ST2 cells had been maintained in normal proliferation media or PROe media since the cell isolation and were designated ST2 and ST2e, respectively. The 12-well plate was place on a Live Cell Imaging system (Kairos Instruments) which can capture images at different coordinates in the well and in all the seeded wells at preprogrammed time intervals, which can then be viewed after a set time as a time- lapsed movie. In the current experiment 100x images were captured every 15 minutes for a period of 108 hours. Images were analyzed using ImageJ and the data are presented in figure 2. Morphologically, the ST2e cells (2B) are smaller and less elongated than the ST2 cells and proliferate at a faster rate than ST2 cells (2C). Next, we wanted to know if the cells were able to differentiate after culture in PROe media and to compare this to cells grown under

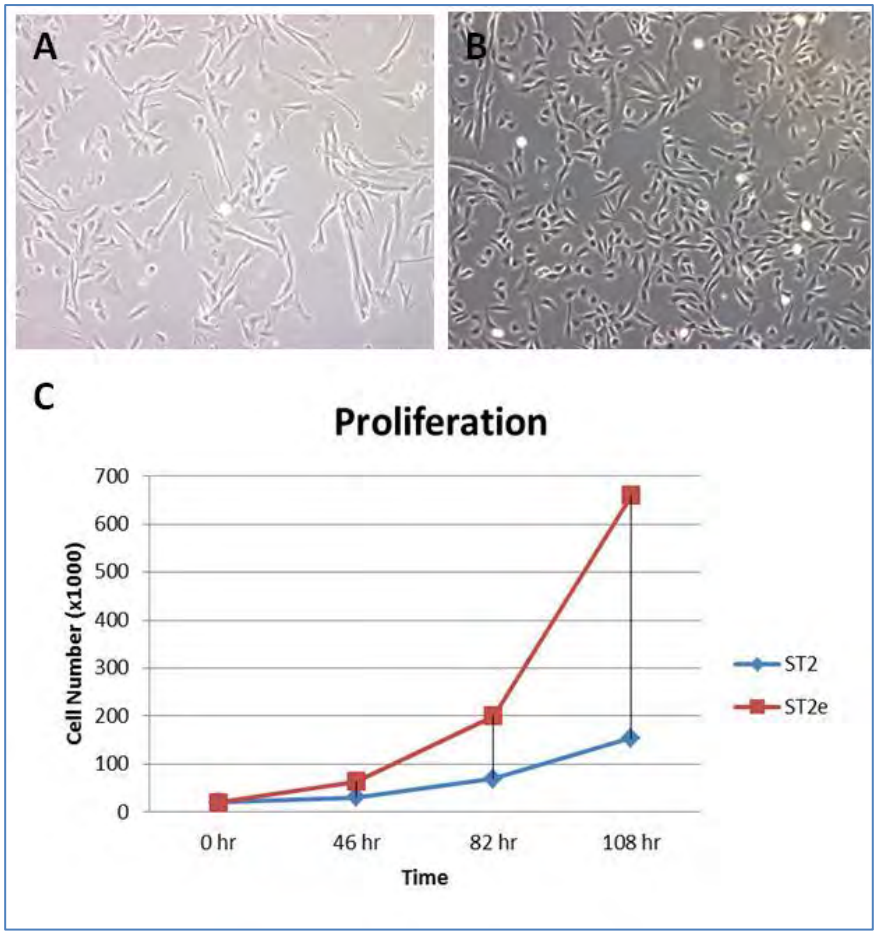

Figure 3: 100x images of human, male myoendothelial cells cultured in PRO media or PROe media. The expected doubling time of 24-36 hours is seen in the ST2 population while the ST2e cells show a doubling time of less than 24 hours (C). The morphologies of the cells are shown in A and B and indicate PROe media maintains the population in a more stem-like morphology.

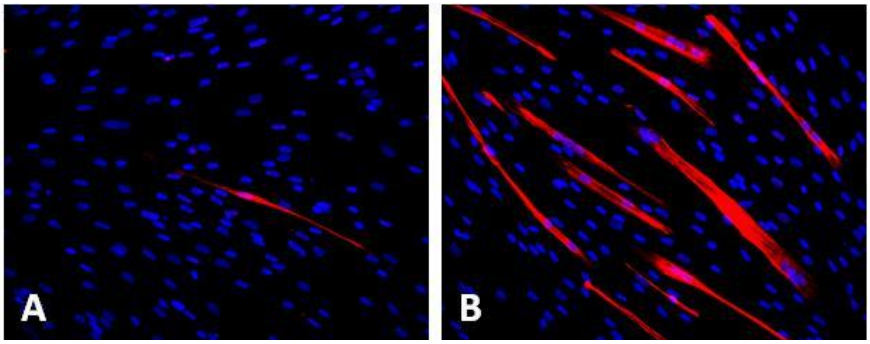

Figure 4: ST2 cells (A) and ST2e cells (B) growth in low (2%) serum media for 5 days. Cells were fixed and stained against DAPI (blue) and myosin heavy chain (red).

the usual culture conditions (PRO). A myogenic differentiation assay was performed, as described above, and representative images are shown in figure 3. ST2e cells not only form a greater number of myotubes but a greater number of the myotubes contained more nuclei which indicate a higher degree of maturity. These data suggest the PROe media or another variant may be more ideal for culturing human myoendothelial cells and maintaining them in a stem-like state.

Identification of a dystrophin antibody for use in mdx mice

Early analysis of the first mdx/SCID tissues transplanted with human myoendothelial cells revealed a critical problem. Our group was using a polyclonal anti-dystrophin antibody (Abcam #15277) which we use for all our other mouse tissues. The initial staining of the mdx/SCID tissues showed high levels of positive staining in the PBS injected control muscles which should have been completely negative (figure 5C-D). Indeed the PBS groups had higher levels of dystrophin staining than some of the tissues tissues injected with myoendothelial cells (5A-B). It was essential to identify a viable anti-dystrophin antibody to stain *mdx* mouse tissues. Dr. Bing Wang of the Stem Cell Research Center had created four variants (R1R2, R2N, R22R23, R24H4) of a mammalian dystrophin antibody for testing on these tissues. The results shown in figure 5 suggested variant R1R2 was the best antibody to use on the *mdx/SCID muscle* tissues (Figure 6).

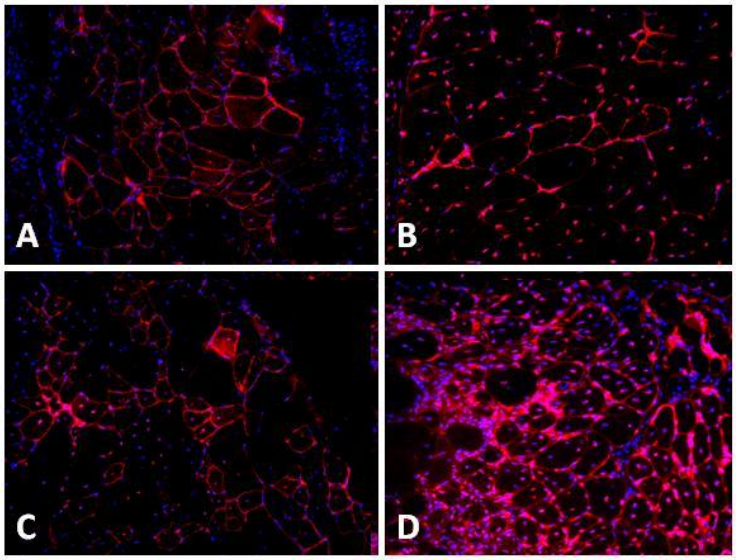

Figure 5: Mdx/SCID muscle sections stained against DAPI (blue) and mammalian dystrophin (red). (A-B) tissue transplanted with human myoendothelial cells. (C-D) tissue injected with PBS.

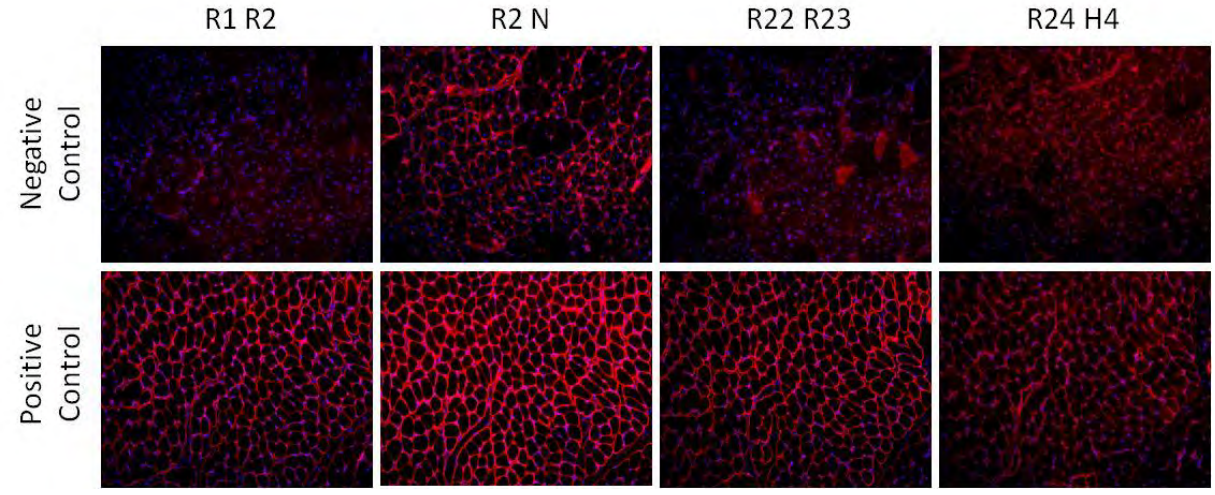

Figure 6: Testing the 4 variants of Dr. Bing Wang's polyclonal dystrophin antibody. Negative control = mdx tissue. Positive control = C57BL6 tissue. Each figure for negative or positive controls shows the identical area of the tissue. Variant R1R2 shows the lowest level of nonspecific staining.

Effect of host sex on the regenerative capacity of old male and female myoendothelial cells

Eight week old mdx/SCID mice, male and female, were randomly assigned to 1 of 5 groups; non-injected (controls), PBS (controls), ST2, ST2e or HM49. All groups, except non-injected controls, received bilateral injections into the gastrocnemius muscles of 20 microliters of PBS or PBS containing $3x10^5$ myoendothelial cells via a 31 gauge insulin syringe. Animals were sacrificed and tissue collected 14 days post-injection. Tissues were cryosectioned and the sectioned tissues stained for dystrophin using the R1R2 variant. Analysis was performed by capturing 100x fluorescent images of the entire stained section and counting the number of positively-stained (for dystrophin) fibers present in the section. The data in figure 7 are not complete as analysis has just begun on these tissues but early evidence suggests ST2 cells (cultured in PRO media) have a greater regenerative capacity than cells grown in PROe media (ST2e). The ST2 (69 year old, male) cells showed no differences when transplanted into male or female hosts (n=3 for both). The trend for ST2e cells is for better regeneration when transplanted into female hosts but the n is low for both conditions (male host, n=1; female

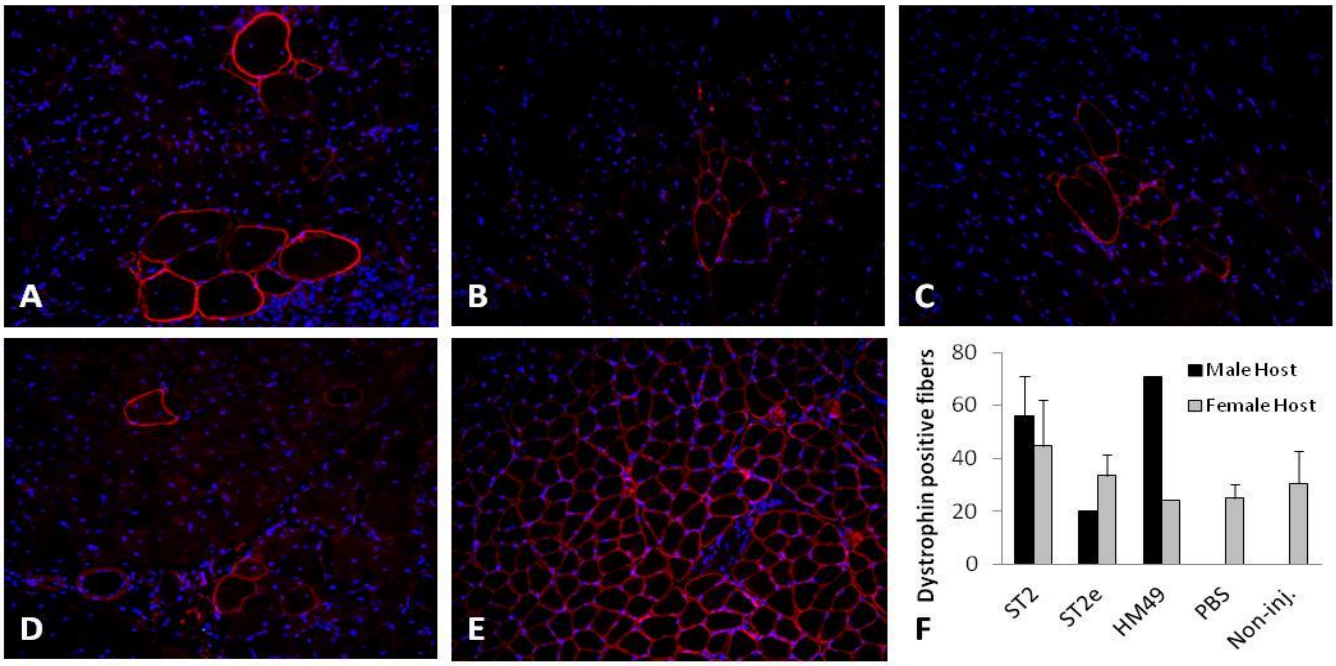

Figure 7: Analysis of tissue cryosections from *mdx/SCID* mice. Dr. Bing Wang's R1R2 dystrophin antibody (red) was used for staining. DAPI (blue) stained for nuclei. A) ST2 injected. B) ST2e injected. C) HM49 injected. D) PBS injected E) wild type (dystrophin positive) control tissue. No significant differences are seen between groups but analysis of tissues is not complete.

host, n=2). This trend is seen in the HM49 again with the HM49 (75 year old, female) injected tissues as greater regeneration is seen when the cells are transplanted into a male host. Again, the n is small (n=1 for both hosts) making further analysis essential for any conclusions to be drawn. More importantly, the numbers of dystrophin positive fibers in female host tissues are all at near-background levels based on the number of revertant myofibers seen in non-injected controls. Analysis has not been performed on non-injected tissues from male hosts. Also, analysis has not yet been performed on non-injected tissues from male hosts.

Non-invasive behavioral testing to detect functional improvement following stem cell transplantation

Preliminary studies were performed on nine, 12-week old female *mdx/SCID* mice in order to test the potential use of a DigiGait™ system (Mouse Specifics, Inc., Quincy, MA) functional gait analysis system to test the functional improvement of our transplanted mice. The mice received bilateral intramuscular (gastrocnemius) injections of 20uL of PBS or 20uL PBS containing either $3x10^5$ male myoendothelial cells or $3x10^5$ male perivascular cells. This initial experiment was conducted before the determination that myoendothelial cells were the best human cell type for these studies. For non-invasive analysis of muscle function we used the DigiGait™ system (Mouse Specifics, Inc., Quincy, MA). The system consists of a treadmill with a transparent belt which had a high speed digital camera mounted ventral to the test subject. Proprietary software provide by Mouse Specifics used to analyze numerous indices of the animal's gait. A simple schematic of what the software is looking at when calculating these indices is shown in figure 8A. For our study animal gaits were examined at a velocity of 20cm/s and the ratio of the stance time to swing time was calculated. The stance and swing phases are shown in figure 8A and the analysis for the *mdx/SCID* mice is shown in 8B. The data suggest that within 2 weeks of transplantation the myoendothelial-injected mice showed a reduced "running" stride compared to the pericyte-injected mice. Since these mice were forced to move at a constant velocity subjects capable of generating more force via plantar flexion could have a ratio of stance/swing greater than 1. Since the gastrocnemious is partially responsible for plantar flexion and this muscle was the target of the transplantation, these data are encouraging and warrant further use with our other experimental animals.

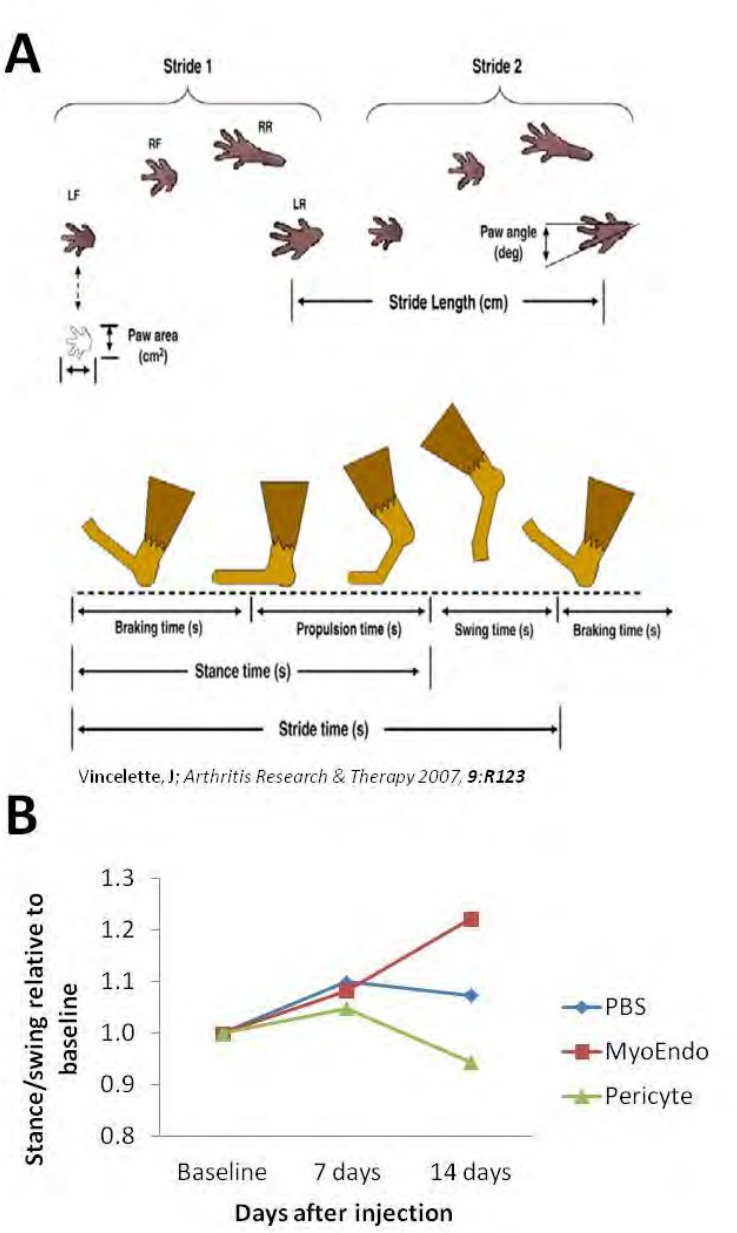

Figure 8: Non-invasive behavioral testing A) schematic of the paw areas detected by the high-speed camera as part of the DigiGait™ system. The diagram below is a visual representation of the 3 phases of a stride; braking, propulsion and swing. B) The stance phase/swing phase ratio for each group at each time point relative to each groups' baseline ratio. An increasing ratio may be indicative of increased muscle function/strength.

Immunomodulatory properties of muscle-derived stem cells associated with reduced NF-κB/p65 signaling

In this study, we examined the role of NF-kB signaling in the regenerative phenotype of muscle-derived stem cells (MDSCs) isolated from the gastrocnemius of p65 deficient mice (heterozygous, *p65*+/-) and wild type littermates (*p65*+/+). We previously found that *p65*+/- MDSCs have enhanced cell proliferation, survival under oxidative stress, differentiation, and muscle regeneration capacity. Furthermore, we have found that *p65*+/-

engraftments in wild type skeletal muscle are associated with reduced inflammation and fiber necrosis compared to *p65*+/+ MDSC engraftments. *In vitro* and *in vivo* experiments suggest that reduction of p65 signaling enhances the regenerative phenotype of MDSCs, suggesting this pathway as a candidate target to improve stem cell-based therapies for muscle disease and injury. The data presented in this study provides evidence supporting that NF-kB inhibition stimulates MDSC-mediated muscle regeneration through multiple mechanisms, including through the expression of anti-inflammatory factors that attenuate inflammation and necrosis. These experiments identify the NF-κB signaling pathway as a potential therapeutic target to enhance muscle regeneration following injury or disease (**Paper in revision. A. Lu et al. Mol. Therapy, Sept. 2011**).

p65 +/- MDSC transplantation improves muscle histology in dKO mice after IP transplantation (Figure 9) -- MDSCs were isolated from 5 month old $p65^{+/-}$ and WT mice as previously described via a modified preplate technique. A total of 5-9 $x10^5$ viable cells or 50µl PBS were injected intraperitoneally into 5-7 day old dKO mice. Four to six weeks after transplantation, the muscles were harvested and cryosections were prepared for staining. Our preliminary data suggest that the regeneration of both the gluteus maximus and diaphragm muscles were more greatly improved in their histopathological appearance in the animals injected IP with p65-deficient MDSCs than the nontreated animals at 4 weeks post-implantation,.

Figure ~~14~~9

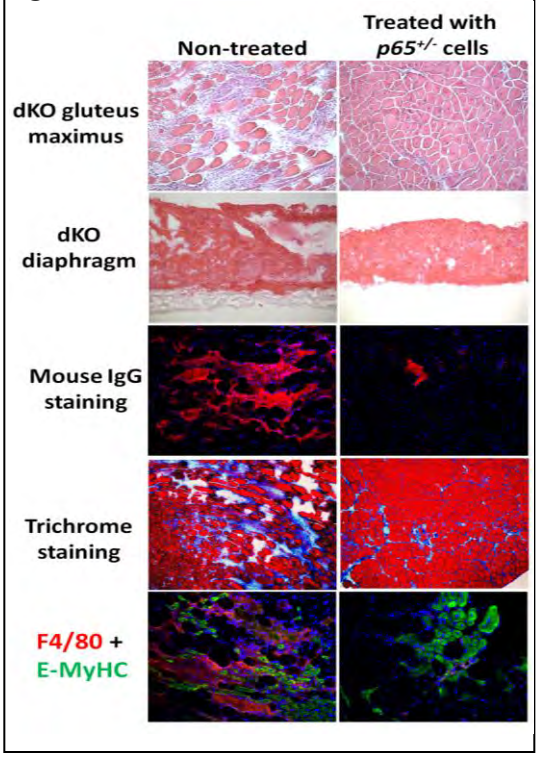

Muscle cryosections were also stained for mouse IgG to determine the extent of muscle fiber necrosis.The results showed that there were less necrotic muscle fibers in the mice injected with $p65^{+/-}$ MDSCs compared to non-treated muscles (**Fig. 9**). Trichrome staining was also preformed according to the manufacturer's instructions and the results showed that there was less muscle fibrosis in the mice injected with $p65^{+/-}$ MDSCs compared to the non-treated muscles (PBS) (**Fig. 9**)

An antibody against embryonic muscle heavy chain (E-MyHC) was used to evaluate muscle regeneration and another antibody against F4/80 (macrophage marker) was used to analyze the extent of inflammation in the regenerated area. These results showed less inflammation (red, F4/80) within the regenerated area (E-MyHC (green) positive myofibers) in the muscles of mice injected with $p65^{+/-}$ MDSCs compared to the untreated muscles (**Fig. 9**). The use of NF-kappa blockade may be useful to improve the regeneration index of hMDCs in the skeletal muscle of MDX/SCID mice.

Progress made from 9-1-09 to 8-31-10

The overall goal of Technical Objective 1 is to identify the optimal human muscle derived cell type for skeletal muscle regeneration. We have completed several aspects of Technical Objective 1, namely – 1)

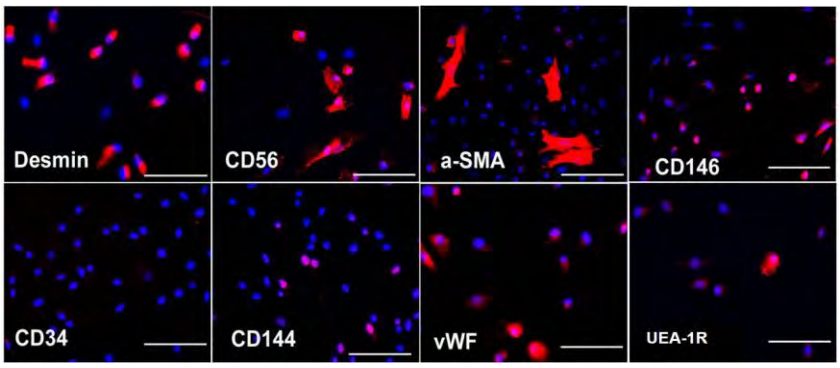

Figure 1. Differential expressions of myogenic and endothelial markers by cryopreserved human skeletal muscle cells. Immunocytochemistry revealed the diverse expressions of various cell lineage markers by cryopreserved skeletal muscle cells after expansion. Nuclei were stained blue with DAPI. (Scale bars = 100µm).

isolation of FACS-defined populations of myoblasts, myo-endothelial cells and pericytes, 2) side-by-side comparison of in vitro myogenic differentiation potential of these populations and 3) transplantation of these 3 populations to mdx/SCID animals and in vivo assessment of skeletal muscle regeneration potential of these cells.

After expansion, the cryopreserved human progenitor skeletal muscle cells (cryo-hPSMCs) were examined by immunocytochemistry for cell surface marker expression. The majority of the cryopreserved skeletal muscle cells expressed desmin and CD56, and to a lesser extent, CD146 (Figure 1). Only a fraction of cells expressed α-SMA, CD144, vWF or UEA-1R. As expected with cultured human cells, cells lacked CD34 expression. Our flow cytometry analysis quantitatively confirmed the diverse expressions of cell lineage makers by the cells: 77.1±5.7% $CD56^+$, 66.9±8.1% $CD146^+$, 11.2±2.5% UEA-$1R^+$, 0.3±0.1% $CD144^+$, 0.1% vWF^+, and no expression of CD34 and KDR (Figure 2A). Surprisingly, the number of cryo-hPSMCs positive for CD56, CD146 or UEA-1R decreased dramatically after passage 10 as compared to expression prior to passage 10 (Figure 2B).

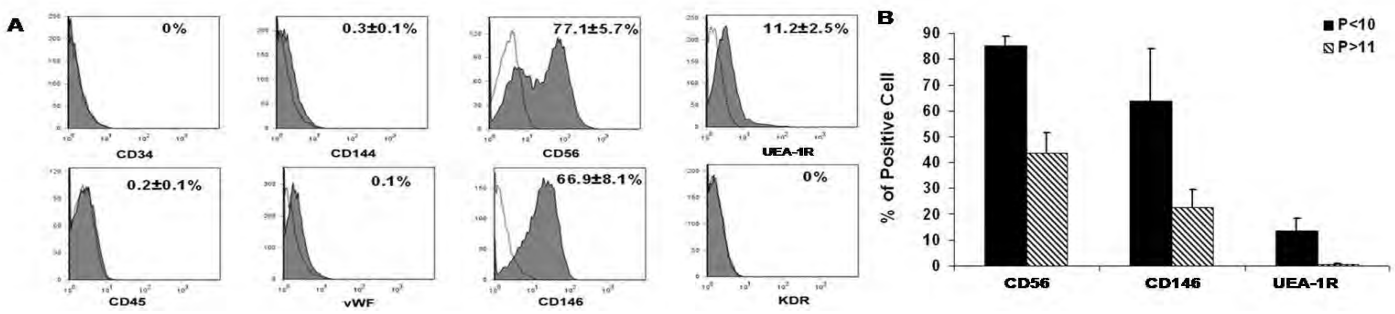

Figure 2. Differential expressions of myogenic and endothelial markers by cryopreserved human skeletal muscle cells. (A) Flow cytometry analysis quantitatively confirmed the diverse cell composition of cryopreserved skeletal muscle cells (B) The number of cryopreserved skeletal muscle cells positive for CD56, CD146, or UEA-1R decreased dramatically when cells were cultured beyond passage 10 (passage>10).

Isolation of myogenic stem/progenitor cells: Using a collection of cell lineage markers, we analyzed cryopreserved cells by flow cytometry for their expression of hematopoietic (CD45), myogenic (CD56), endothelial (UEA-1R), and perivascular (CD146) cell markers. After the exclusion of $CD45^+$ cells, four distinct cell fractions were identified, including myoblasts (Myo) ($CD56^+/CD45^-CD146^-$UEA-$1R^-$), endothelial cells (ECs) (UEA-$1R^+/CD45^-CD56^-CD146^-$), perivascular stem cells (PSCs) ($CD146^+/CD45^-CD56^-$UEA-$1R^-$), and myogenic endothelial cells (MECs) which expressed all three cell lineage markers ($CD56^+$UEA-$1R^+CD146^+/CD45^-$). The composition of long-term cultured cryopreserved muscle cells included 22.58±6.32% Myo, 0.58±0.23 % ECs, 5.92±4.66% PSCs, and 1.16±0.19% MECs (Figure 3). These four cell subsets were subsequently fractionated by FACS (Figure 3).

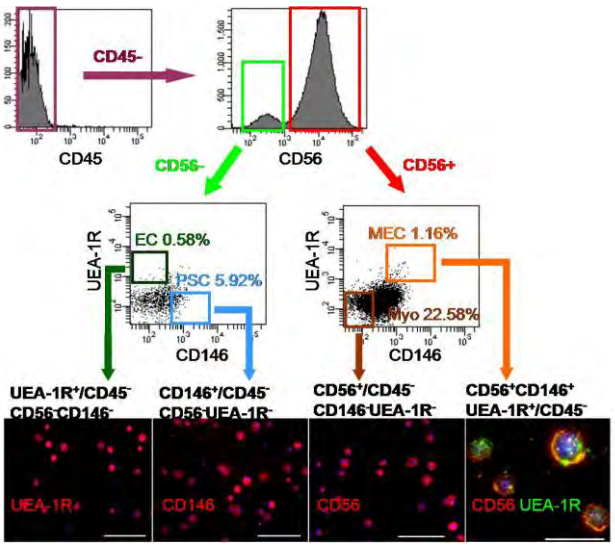

Figure 3. Identification and purification of myogenic stem cells within cryopreserved muscle cell populations. $CD45^-$ cells were separated based on CD56 expression. $CD56^+$ and $CD56^-$ populations were further gated on UEA-1R by CD146 to identify and/or sort four distinct cell populations: myogenic endothelial cells (MEC) ($CD56^+UEA\text{-}1R^+CD146^+/CD45^-$), myoblasts (Myo) ($CD56^+/CD45^-CD146^-UEA\text{-}1R^-$), perivascular stem cells (PSC) ($CD146^+/CD45^-CD56^-UEA\text{-}1R^-$), and endothelial cells (EC) ($UEA\text{-}1R^+/CD45^-CD56^-CD146^-$). The purities of the sorted populations were 90.73±4.82%, 92.94±1.23%, 93.86±1.72, and 94.9±0.64, respectively. Immunocytochemistry confirmed the expression of key cell lineage makers by freshly sorted cells: UEA-1R, CD146, and/or CD56. (Scale bars = 100µm except in CD56/UEA-1R double staining = 20µm)

Next, we examined the in vitro differentiation capacity of myoendothelial cells and pericytes. Cells were stimulated for 1 week under conditions of low serum and high density and we observed a marked difference in the ability to undergo myogenic differentiation, as noted by the presence of multinucleated myotubes and positive immunostaining for myosin heavy chain (MHC) and desmin (Figure 4).

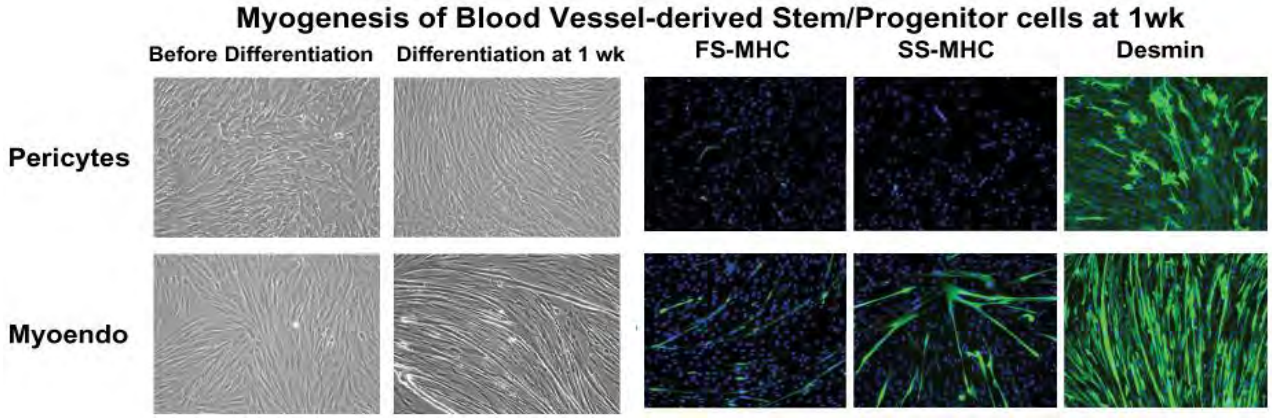

Figure 4. Myoendothelial cells displayed a higher myogenic potential as compared to pericytes. After 1 week in myogenic conditions, we find more myotubes, and greater expression of myosin heavy chain (MHC, green) and desmin (green) in the myoendothelial cell populations as compared to pericytes populations. Nuclei are DAPI stained.

Finally, to evaluate the myogenic capacities of these purified cell fractions, all freshly sorted cells were immediately transplanted into cardiotoxin-injured skeletal muscles of SCID mice (n=7 per cell fraction). Unpurified muscle cell- and saline-injected muscles were employed as controls. Mouse muscles were harvested 2 weeks post-injection, cryosectioned, and examined by immunohistochemistry to detect muscle fiber regeneration *in vivo*. An antibody against human spectrin, a myofiber cytoskeletal protein, was used to identify human cell-derived skeletal myofibers in the tissue sections. Quantitative analyses revealed that the myogenic regeneration index, indicated by human spectrin-positive skeletal myofibers per 1×10^3 injected cells, was

71.23±27.15 for MECs, 31.26±11.57 for endothelial cells (ECs), 11.44±3.79 for PSCs, 4.23±1.16 for myoblasts (Myo), and 0.55±0.36 for unsorted muscle cells (Unsort) (Figure 4). MECs exhibited the highest regeneration of human skeletal myofibers among all five cell fractions tested ($p<0.05$) (Figure 4). PSCs regenerated more myofibers than the Myo ($p>0.05$) and the Unsort ($p<0.05$) (Figure 5). Purified myoblasts displayed a higher myogenic capacity than the unsorted cells ($p<0.05$) (Figure 5).

Similar experiments are currently under way where the cell populations have been transplanted into the gastrocnemius muscles of mdx/SCID mice – a mouse model of Duchenne muscular dystrophy that is dystrophin deficient and also is immune deficient to inhibit the rejection of the injected human cell populations. These in vivo experiments will allow us to compare the myogenic potential of the cells in a DMD model verse the acute muscle injury model used above (i.e., the cardiotoxin injured mice).

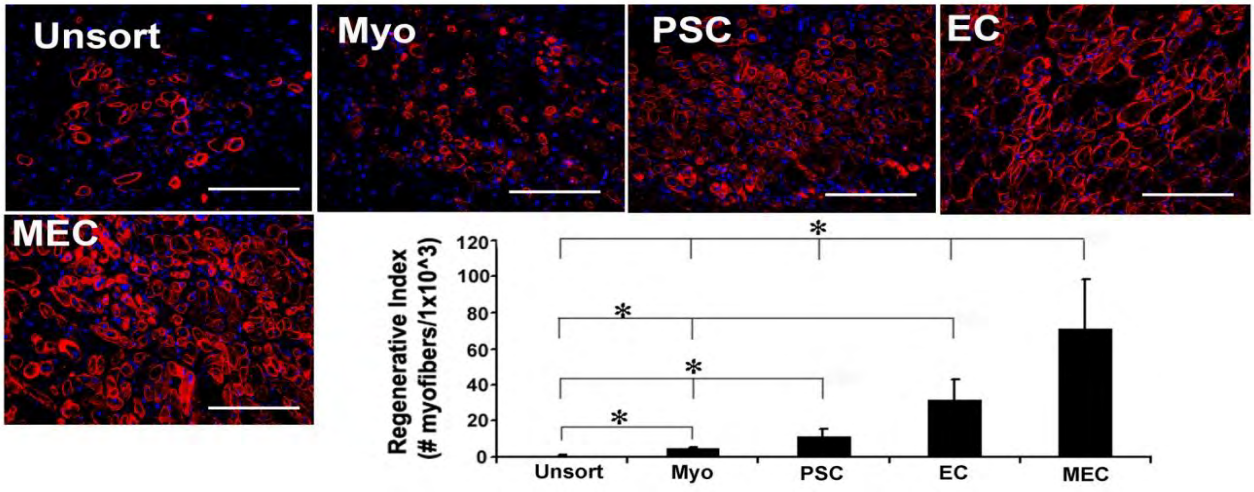

Figure 5. Comparison of myogenic regenerative capacities *in vivo*. Freshly sorted cells were transplanted into the cardiotoxin-injured skeletal muscles of SCID mice. Quantitative analyses of human spectrin-positive skeletal myofibers on tissue sections revealed that myogenic endothelial cells (MEC) mediated the highest myogenic regeneration among all five cell fractions tested (* $p<0.05$). Injection of perivascular stem cells (PSC) regenerated more human myofibers than injections of myoblasts (Myo) ($p>0.05$) and unpurified muscle cells (Unsort) (* $p<0.05$). Finally, myoblasts (Myo) displayed a higher myogenic capacity than unpurified muscle cells (Unsort) (* $p<0.05$). (Red immunostaining is spectrin, Blue nuclei are DAPI stained)

KEY RESEARCH ACCOMPLISHMENTS:

- Demonstration of prospective isolation of myoblasts, pericytes and myo-endothelial cells derived from human skeletal muscle biopsy, and from both expanded and cryopreserved populations.
- Demonstration that the myo-endothelial cells show a higher level of myogenic potential in vitro as compared to myoblasts and pericytes.
- Demonstration that both expanded and cryopreserved cells continue to show some myogenic potential in vitro.
- Demonstration that the myo-endothelial cells show a significantly higher level of skeletal muscle regeneration in vivo as compared to myoblasts and pericytes.
- Obtained preliminary evidence that PP3 cells isolated from young female skeletal muscle has a higher myogenic capacity than PP3 cells isolated from old skeletal muscle.
- Obtained preliminary evidence that myoendothelial cells isolated from young skeletal muscle is more resistant to the effects of oxidative stress than those isolated from old skeletal muscle.

- Preliminary evidence that young and old myondothelial cells possess a similar proliferation capacity.
- Optimized the growth medium for human myoendothelial cells in order to increase their proliferation rates and reduce their differentiation rates by maintaining their stem-like state in culture.
- Identified an antibody that could be used without significant background staining in our mdx/SCID model of DMD.
- Initiated studies comparing male and female myoendothelial regeneration efficiencies in vitro.
- Identified a physiological testing system (DigiGait system) that could give us excellent physiologic readouts of our transplanted animals.
- Immunomodulatory properties of muscle-derived stem cells are associated with reduced NF-κB/p65 signaling.
- p65 +/- MDSC transplantation can improve muscle histology in dKO mice (mice deficient for both utrophin and dystrophin) after IP transplantation.

REPORTABLE OUTCOMES:

1. Aiping Lu, Jonathan Proto, Lulin Guo, Ying Tang, Mitra Lavasani, Jeremy S. Tilstra, Laura J. Niedernhofer, Bing Wang, Denis C. Guttridge, Paul D. Robbins, Johnny Huard J.H. **NF-kappa B Negatively Impacts the Myogenic Potential of Muscle-Derived Stem Cells**, Molecular Therapy Sept. 2011**, Under Revision. (Appendix 1)**

2. Aiping Lu, Qing Yang, Minakshi Poddar, Bing Wang, Denis C. Guttridge, Paul D. Robbins, Johnny Huard; **Transplantation of p65 Deficient Stem Cells Improved the Histopathology of Skeletal Muscle in Dystrophic Mice.** Orthopaedic Research Society; 2011 ORS Annual Meeting; January 13-16, 2011; Long Beach, CA. **(Appendix 2)**

3. Proto, J., Lu, A., Robbins, P.D., Huard, J; **Immunomodulatory properties of muscle-derived stem cells associated with reduced NF-κB/p65 signaling.** Orthopaedic Research Society; 2011 ORS Annual Meeting; January 13-16, 2011; Long Beach, CA. **(Appendix 3)**

4. Bo Zheng, Chien-Wen Chen, Guangheng Li ,Bruno Péault, Johnny Huard; **Prospective Isolation Of Vascular Myogenic Stem Cells From Cultured and Cryopreserved Human Skeletal Muscle Cells;** Cell Transplantation, **In Press.**

5. Bo Zheng, Guangheng Li, Bridget M Deasy, Jonathan B Pollett, Bin Sun, Lauren Drowley, Burhan Gharaibeh, Arvydas Usas, Alison Logar, Bruno Peault , Johnny Huard; **Clonal Analysis of Human Myoendothelial Cells Reveals Stem Cell Characteristics.** In preparation.

6. Chen C, Okada M, Tobita K, Crisan M, Péault B, Huard J; **Transplantation of Purified Human Skeletal Muscle-Derived Pericytes Reduce Fibrosis in Injured Ischemic Muscle Tissues**. Orthopaedic Research Society; March 6-9, 2010; New Orleans, La.

CONCLUSION:

Our results to date show that even after *in vitro* expansion and cryopreservation, primary human muscle cells harbored various subpopulations of cells. We have identified and purified to homogeneity four distinct cell populations from cryopreserved primary human muscle cells including two stem cell subpopulations: Pericytes

(PSCs) ($CD146^+/CD45^-CD56^-UEA\text{-}1R^-$) and myoendothelial cells (MECs) ($CD56^+CD146^+UEA\text{-}1R^+/CD45^-$). Freshly sorted MECs, PSCs, endothelial, and myogenic cells were transplanted into the injured skeletal muscles of SCID mice to examine their myogenic efficacy. MECs displayed the highest muscle regenerative capacity among all cell subsets tested, and PSCs were superior to myoblasts and unpurified cryopreserved primary human muscle cells. These results were consistent with previous observations from the injection of cells isolated from fresh muscle biopsies. Taken together, our results suggest the presence of distinct subpopulations of highly myogenic stem/progenitor cells within expanded cryopreserved primary human muscle cells and support the feasibility of further purifying stem cell fractions from cryopreserved human cells. Most importantly, these findings infer the practicability of prospective isolation of myogenic stem/progenitor cell populations from banked human skeletal muscle cells, highlighting a new technology to further enhance the availability and efficacy of cell-mediated therapies.

We have preliminary evidence that there are no differences in the proliferative abilities between old and young human muscle derived cells; however there does appears to be a difference in their myogenic differentiation capacity and resistance to oxidative stress. We have also formulated a medium that optimizes the proliferative capacity of our human muscle derived stem cells while reducing their premature myogenic differentiation. We have also identified a non-invasive behavioral testing system to detect the functional physiological improvements of the muscles that have been transplanted with our muscle derived stem cells.We have also demonstrated that NF-κB inhibition stimulates MDSC-mediated muscle regeneration through multiple mechanisms, including through the expression of anti-inflammatory factors that attenuate inflammation and necrosis. These experiments identify the NF-κB signaling pathway as a potential therapeutic target to enhance muscle regeneration following injury or disease. Moreover, our current results have demonstrated less inflammation within the regenerating areas of muscles of mice injected with $p65^{+/-}$ MDSCs (MDSCs with ½ the expression of the NF-κB sub unit p65) compared to the untreated muscles (**Fig. 9**); hence the use of NF-kappa blockade may be useful to improve the regeneration index of human muscle-derived stem cells in the skeletal muscle of MDX/SCID mice and potentially in the skeletal muscle to DMD patients.

REFERENCES:

N/A

APPENDICES:

Refer to Manuscripts/Reprints, Abstracts Section

MANUSCRIPTS/REPRINTS, ABSTRACTS:

1. Bo Zheng, Chien-Wen Chen, Guangheng Li ,Bruno Péault, Johnny Huard; **Prospective IsolationOf Vascular Myogenic Stem Cells From Cultured and Cryopreserved Human Skeletal Muscle Cells;** Cell Transplantation, **In Press**.
2. Bo Zheng, Guangheng Li, Bridget M Deasy, Jonathan B Pollett, Bin Sun, Lauren Drowley, Burhan Gharaibeh, Arvydas Usas, Alison Logar, Bruno Peault , Johnny Huard **Clonal Analysis of Human Myoendothelial Cells Reveals Stem Cell Characteristics.** Under Preparation.
3. Chen C, Okada M, Tobita K, Crisan M, Péault B, Huard J. **Transplantation of Purified Human Skeletal Muscle-Derived Pericytes Reduce Fibrosis in Injured Ischemic Muscle Tissues**. Orthopaedic Research Society; March 6-9, 2010; New Orleans, La.

Sub-Project 2: Generation of human hepatocytes from patient-specific stem cells for treatment of life-threatening liver injury

PIs: David Perlmutter and Ira J. Fox

INTRODUCTION:

These studies are focused on generating human hepatocytes from patient-specific stem cells for the treatment of life-threatening liver injury. Two technical objectives were proposed: 1) Determine the extent to which human patient-specific, inducible pluripotent stem (iPS) cells can be differentiated into primary human hepatocytes, and 2) Determine the extent to which the PiZ mouse model of alpha-1-antitrypsin (AT) deficiency can be developed as a platform for pre-clinical testing of hepatic stem cell transplantation as a treatment for severe liver injury and disease. In order to accomplish these objectives, we have continued to generate human iPS cell lines from normal patients and, more directly, from patients with alpha-1-antitrypsin deficiency. These cells have now been characterization and we are differentiating them into hepatocytes. We have demonstrated that hu-iPS derived cells can be transplanted in rodents that are models of human disease and that engraftment and expansion of the derived hepatocytes corrects the disease. Finally, we have further determined the ability of donor hepatocytes to expand in the PiZ mouse, and we have generated PiZ mice on an immune-deficient background and have begun studies showing engraftment and expansion of pluripotent stem cell-derived hepatocytes in these mice.

BODY:

1.1 Generation of human induced pluripotent stem cells (hu-iPS cells)

We hypothesized that patient specific iPS cells could be generated from primary human cells, including hepatocytes, and that under appropriate conditions, the iPS cells could be induced to differentiate back to hepatocytes that could be used as cellular therapy to treat the liver defect. Here, we report the generation of multiple human iPS cell lines from primary human cells following exposure to either lentiviral or retroviral constructs carrying the reprogramming factors. In Table 1, we characterize lines only derived from

Table 1. List of control and AATD iPS cell lines

Source of iPS cell line	Normal human hepatocyte (patient)	Normal lung fibroblast (ATCC)	Normal dermal fibroblast	A1AT deficient human hepatocyte (Biopsy)	A1AT deficient lung fibroblast (Biopsy)	A1AT deficient hepatic fibroblast (Coriell)
Vector used for iPS induction	Aruna lentivirus	Yamanaka retrovirus	Yamanaka retrovirus	Aruna lentivirus	Aruna lentivirus	Yamanaka retrovirus
Charcterization of Pluripotency						
qPCR	✓	✓	✓	✓	Not done	✓
Immunostaining	✓	✓	✓	✓	Not done	✓
Teratoma formation	✓	✓	✓	✓	Not done	✓

Genotype*	Not done	Not done	Not done	A/A	A/A	A/G
Name of iPS cell line	**HH1591** iPS cells (Control)	**IMR90** iPS cells (Control)	**YU** iPS cells (Control)	**ATH-1** iPS cells (A1AT deficient)	**AT-10** iPS cells (A1AT deficient) 8 clones	**GM-1-1** **GM-2-1** iPS cells (A1AT deficient)

*** A/A: Homozygous for the Z allele; A/G heterozygous for the Z allele**

normal controls, and patients with alpha-1-antitrypsin deficiency (AATD). We have characterized the lines for markers of pluripotency, including alkaline phosphatase activity, nuclear OCT4 staining and reactivity to antibodies to the surface markers SSEA-3, SSEA-4, TRA1-60, and TRA1-81, and confirmed these results by qPCR. In addition, genotyping has been completed on those lines derived from patients with AATD.

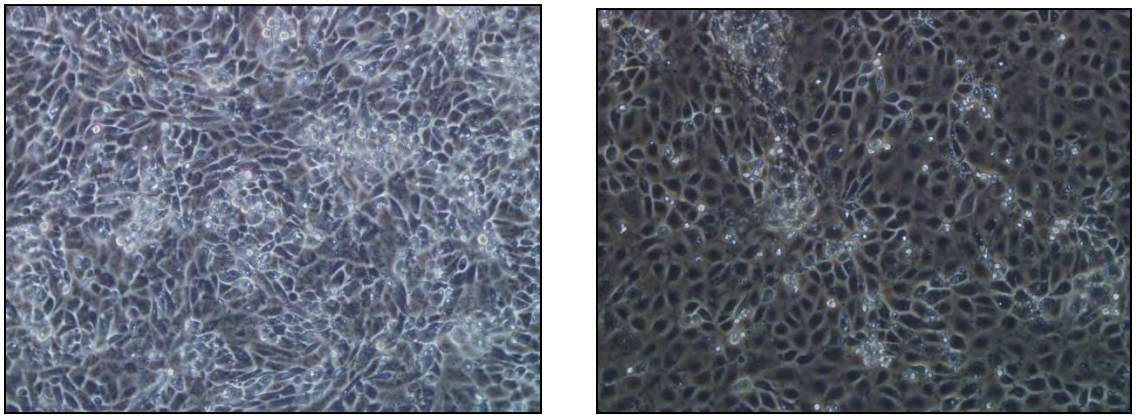

Figure 1. Morphologic changes during iPS differentiation. Left, morphology of iPS cells during the phase of definitive endoderm; right, morphology of iPS cells during the hepatic specification phase of differentiation.

1.2. Differentiation of human iPS cells into hepatocytes.

We have now generated iPS-derived hepatocytes in a manner similar to what we have published[1], and using a variation on the technique described by Si-Tayeb [2]. **Figure 1** illustrates the morphologic changes that occur

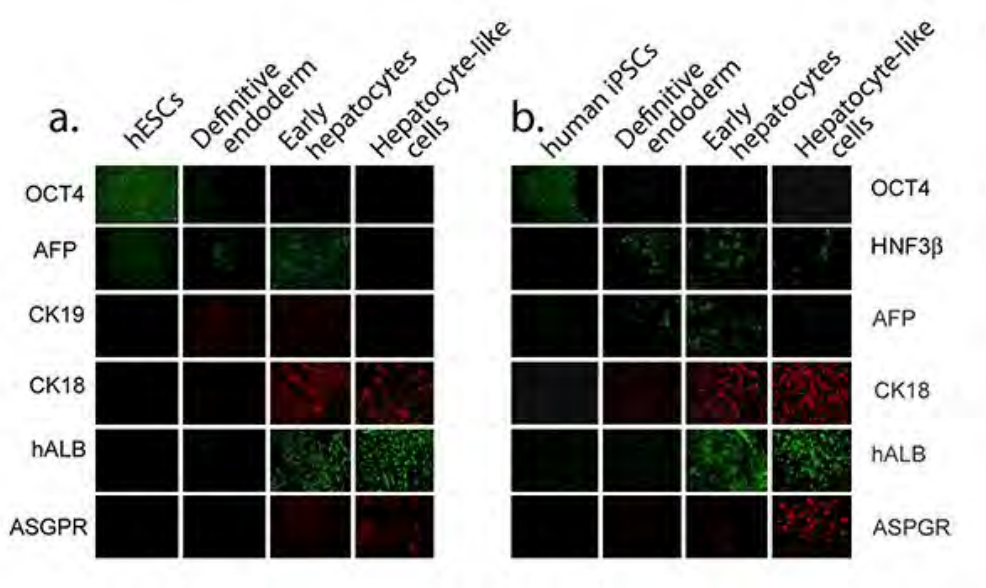

Figure 2. Expression of cellular marker proteins during differentiation of human ES (a) and iPS (b) cells. The ES and iPS cells were differentiated sequentially to definitive endoderm, early hepatocytes and hepatocyte-like cells. Immunofluorescence staining for human OCT4, alpha-fetoprotein (AFP), cytokeratin 19 (CK19), cytokeratin 18 (CK18), hepatic nuclear factor 3β (HNF3β), human serum albumin (hALB) and asialoglycoprotein receptor (ASGPR) are shown.

during differentiation, and **Figure 2** demonstrates changes in the expression profile during various stages of the later differentiation process. Not shown is that after completion of the differentiation protocol, UGT1A1 activity in the cells was 15-20% of that in human liver homogenates. **Figure 3** shows that the differentiated cells secrete more than 20% of the albumin and 30% of the alpha-1-antitrypsin released by primary human hepatocytes.

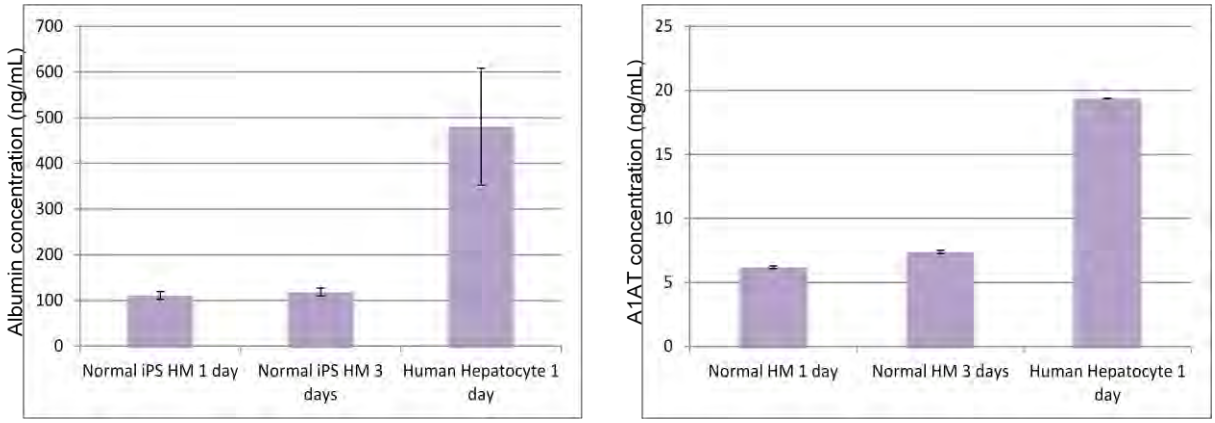

Fig 3. ELISA results following hepatocyte-specific differentiation of control iPS cells.
Shown are the albumin and AAT-specific ELISA measurements derived from the supernatant of iPS cells during the first and 3rd days of the hepatic maturation step during differentiation compared to the results from control fresh primary human hepatocytes.

1.3 Transplantation of human iPS-derived hepatocytes with correction of hyperbilirubinemia in the Gunn rat model of Crigler-Najjar syndrome type 1. To determine the extent to which stem cell-derived human hepatocytes could be engrafted in immune suppressed rat hosts, we transplanted iPS-derived hepatocytes into Gunn rat livers by intrasplenic injection [3]. To provide a proliferative advantage to the transplanted cells,

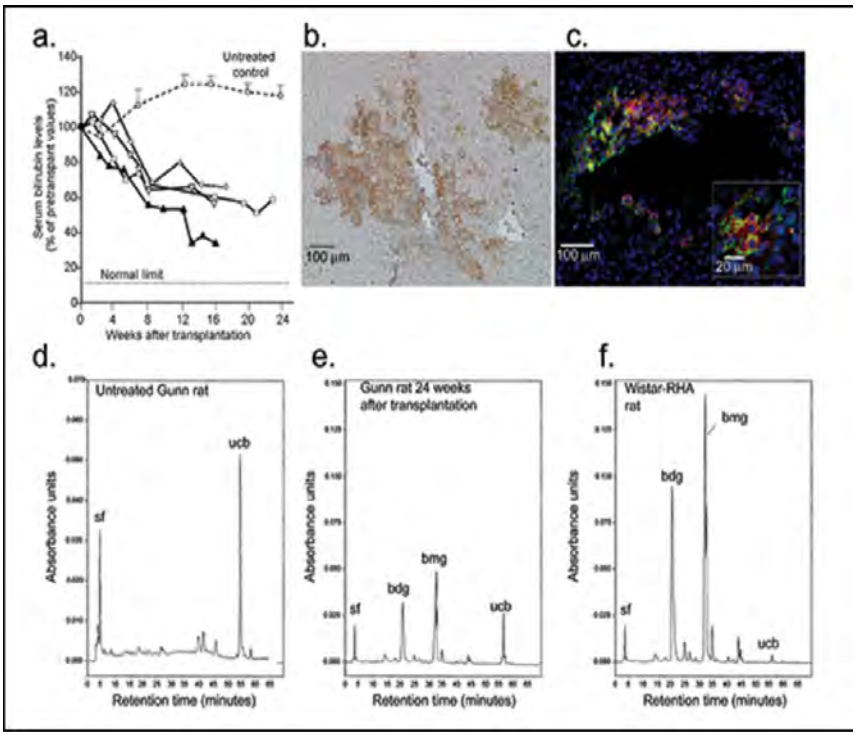

Figure 4. Effect of repopulation of the Gunn rat liver by iPSC-derived hepatocytes. a, Serum bilirubin levels in the four recipient Gunn rats (diamond, square, open and closed triangles) at the indicated time points after transplantation of human iPS cell-derived hepatocytes are shown as percentage of pre-transplantation levels. Bilirubin levels of untreated age-matched controls are also shown (open circles, mean+SEM of 6 rats). The upper limit of serum bilirubin levels in congeneic normal Wistar-RHA rats is shown as a dotted line. b and c, Representative liver sections from a recipient Gunn rat 4-6 months after transplantation of human iPS-derived hepatocytes. b, Immunohistochemical staining for human UGT1A1 showing cell clusters derived from the transplanted cells. c, Dual immunofluorescence staining showed that a majority of cells positive for human serum albumin (green) were also positive for human UGT1A1 (red). The nuclei are stained blue (DAPI). A magnified view is shown in the insert. d-f, HPLC analysis of bilirubin species excreted in the bile of a control Gunn rat, a rat receiving iPS-derived hepatocytes and a congeneic normal Wistar RHA rat is shown. sf, solvent front; ucb, unconjugated bilirubin; bdg, bilirubin diglucuronide; bmg, bilirubin monoglucuronide. Note the difference in the absorbance unit scale in panel c from that in panels d and e.

part of the host liver was irradiated (50Gy) and an adenovirus vector expressing hepatocyte growth factor was injected. For immune suppression, Tacrolimus (2mg/kg) was injected daily beginning 7 days before transplantation. After transplantation, serum bilirubin levels declined, as shown in **Figure 4**, and immuno-histochemistry of liver sections showed clusters of human albumin and UGT1A1-positive cells, and bilirubin conjugates appeared in the bile, indicating function by engrafted, UGT1A1-expressing iPS-derived hepatocytes.

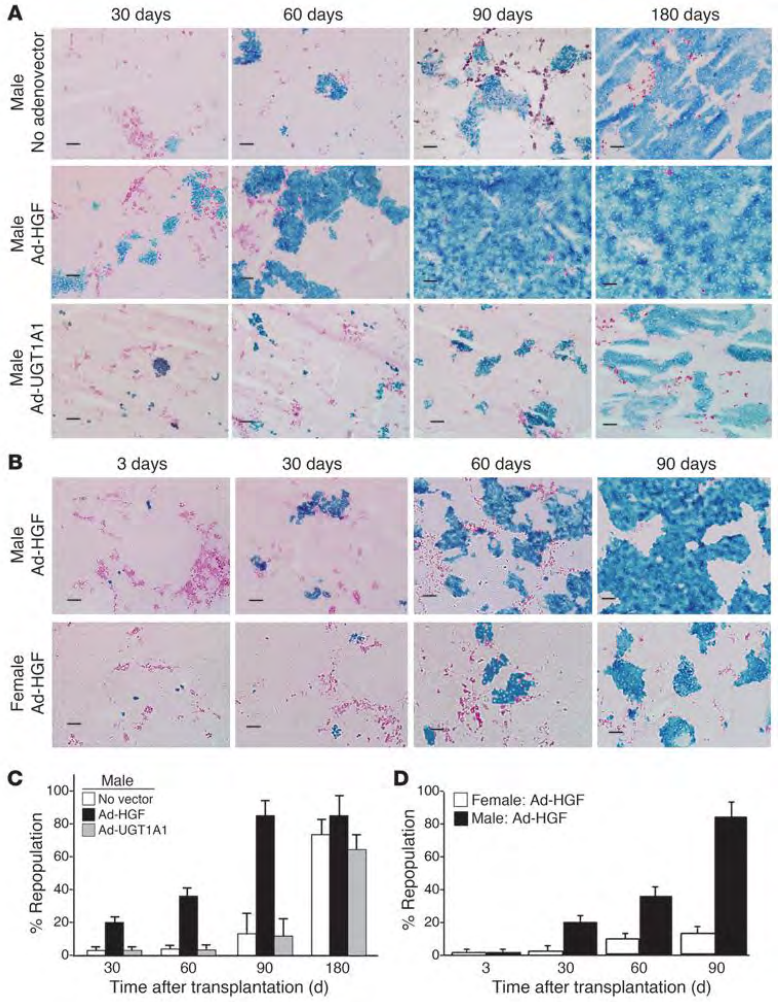

Figure 5. Kinetics of hepatic repopulation in PiZ mice. (A) Ad-HGF administration accelerated repopulation. ROSA26 mouse hepatocytes (1 × 106) were transplanted into male PiZ mice without (upper row) or with (lower row) Ad- HGF (1 × 1011 particles, i.v.). Liver sections were stained for *E. coli* β-gal (blue), and diastase plus PAS (magenta) to visualize AAT-Z globules. Scale bars: 100 μm. Data are from representative mice from each group (n = 6). (B) Repopulation was greater in male recipients. Male and female PiZ mice received Ad-HGF (n = 6). Hepatocyte transplantation and staining of liver sections were as in A. (C and D) Quantitative DNA PCR. Quantitative PCR for the *E. coli lacZ* gene was performed on DNA extracted from livers of recipient mice. Percentage of repopulation was calculated as described in the text. (C) Graphic presentation of data from experimental groups shown in A (mean ± SEM; n = 6 in each group), showing significantly higher repopulation in the Ad-HGF group at all time points (P < 0.05). (D) Data are from the experimental groups shown in B (mean ± SEM; n = 6 in each group), showing significantly higher repopulation in males 30, 60, and 90 days after transplantation (P < 0.05).

1.4. Hepatocyte engraftment and proliferation AT (PiZ) transgenic mice. In several animal models, transplanted hepatocytes have a proliferation advantage over the host liver cells, and nearly 100% of the native liver can be replaced by the donor cells [4, 5]. In AT deficiency, the abnormal Z protein can aggregate in hepatocytes and these aggregates may damage cells. Through this mechanism, AT deficiency patients may develop liver disease. Since Z protein aggregation leads to hepatocyte apoptosis, it has been hypothesized that PiM hepatocytes transplanted into PiZ livers would have a similar selective advantage and may progressively increase their relative contribution to liver mass. To examine this possibility, hepatocytes isolated from ROSA26 (beta-galactosidase transgenic mice) were transplanted into 6-8 week old human AT (hAT) transgenic mice. Three months after transplantation approximately 20% of the native liver was replaced by ROSA26 hepatocytes, as assessed histologically by lacZ staining **(Fig 5)**. These data provide direct evidence, in an animal model, that PiM hepatocytes have the capacity to progressively replace PiZ-expressing hepatocytes following transplantation. In addition, we have accumulated direct evidence that expansion of donor hepatocytes occurs in association with specific areas in the native liver where high levels of the mutant AT protein can be found as aggregates in the host hepatocytes, presumably leading to apoptosis [6].

We then hypothesized that expression of the mutant AAT-Z should reduce the capacity of the host hepatocytes to proliferate in response to mitotic stimuli, which should accelerate repopulation by transplanted wildtype cells. To test this, we examined the extent of hepatic repopulation after hepatocyte transplantation in groups of recipient PiZ mice with administration of Ad-HGF. The extent of repopulation was significantly greater at all time points in the group that received Ad-HGF. A control group that received an adenovector that expressed an irrelevant gene did not exhibit accelerated repopulation. Ninety days after transplantation 40-60% of the hepatocytes were replaced by donor cells, and in occasional PiZ recipients, the repopulation was nearly complete, so that only the bile duct epithelial cells and the non-parenchymal cells remained from the host liver **(Fig 5)**. The increased death rate of host hepatocytes, combined with a greater mitotic activity of the donor cells resulted in progressive repopulation of the host liver by the donor cells, while the liver size remained unaltered.

1.5. iPS-derived human hepatocyte engraftment and proliferation in immune-deficient AT transgenic mice. In last year's report we examined whether human hESC-derived hepatocytes could engraft and proliferate spontaneously in the livers of immune deficient PiZ mice. We have now examined whether iPS-derived hepatocytes can engraft in such animals. We generated SCID/PiZ mice, and the PiZ genotype in the offspring and zygosity for the SCID mutation were determined by PCR and pyrosequencing, respectively. Human iPS cells were then differentiated to hepatocytes as described, and one million cells were transplanted into the livers of SCID/PiZ mice by intrasplenic injection. To stimulate mitosis of hepatocytes, $1x10^{11}$ adenovirus vector particles expressing hepatocyte growth factor (Ad-HGF) were injected IV into recipients one day after transplantation. Engrafted hepatocytes were identified by immunofluorescence staining for human serum albumin (HSA). The engrafted human cells had hepatocyte-like morphology and,
by three months after transplantation, engrafted iPS-derived hepatocytes were present as large colonies within the host liver **(Fig 6)**. Host cells exhibited diastase/PAS-positive AAT-Z globules, but the HSA-positive human hepatocytes did not. These studies indicate that immune deficient PiZ mice are an excellent model for evaluating stem cell-derived human hepatocytes in terms of engraftment, proliferation and function [7].

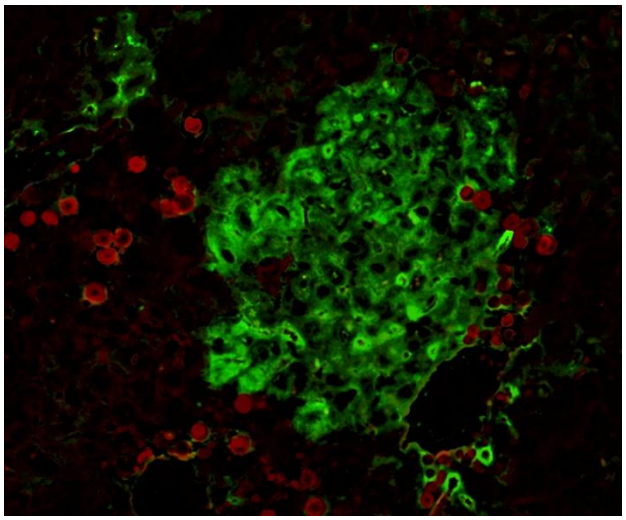

Fig 6. Transplantation of ES-derived human hepatocytes in SCID-PiZ mice. Three-months following transplantation of iPS-derived hepatocytes into immune deficient PiZ mice, immunofluorescence shows large clusters of engrafted iPS-derived hepatocytes stained green for human albumin. Red staining represents hAAT globules in host hepatocytes. Nuclei are stained with Dapi (blue).

KEY RESEARCH ACCOMPLISHMENTS:

1. Generation and characterization of hu-iPS cell lines from control patients and patients with AT-deficiency
2. Further characterization of hu iPS cells during differentiation into hepatocyte-like cells
3. Transplantation and expansion of human iPS-derived hepatocytes in rats, with correction of hyperbilirubinemia in the Gunn rat model of Crigler-Najjar syndrome type 1.
4. Complete repopulation of PiZ mouse livers with allogeneic hepatocytes facilitated by the use of hepatocyte growth factor administration after transplantation

5. Engraftment and proliferation of human pluripotent stem cell-derived hepatocytes in immune-deficient alpha-1-antitrypsin-deficient transgenic mice

REPORTABLE OUTCOMES:

1. Ding J, Yannam GR, Roy-Chowdhury N, Hidvegi T, Basma H, Rennard SI, Wong RJ, Avsar Y, Guha C, Perlmutter DH, Fox IJ, Roy-Chowdhury J. Spontaneous repopulation of the liver of transgenic mice expressing mutant human alpha 1-anti-trypsin by wildtype donor hepatocytes. J Clin Invest 2011;121(5):1930-1934.
2. Roy-Chowdhury N, Chen Y, Atienza K, Chang C, Wang X, Guha C, Fox IJ, Bouhassira EE, Roy-Chowdhury J. Amelioration of hyperbilirubinemia in Gunn rats after transplantation of human hepatocytes derived from induced pluripotent stem cells. J Clin Invest (submitted).
3. Atienza K, Ding J, Chang C-J, Bouhassira E, Chen Y, Wang X, Avsar Y, Liu L, Guha C, Fox IJ, Salido E, JRoy-Chowdhury J, Roy-Chowdhury N. Reduction of urinary oxalate excretion after transplantation of human induced pluripotent stem cell-derived hepatocytes in a mouse model of primary hyperoxaluria-1. AASLD 2011.
4. Ding J, Wang X, Neufeld D, Hansel M, Strom S, Fox IJ, Guha C, Roy-Chowdhury N, Roy-Chowdhury J. SCID/PiZ mice: a novel animal model for evaluating engraftment and proliferation of human stem cell-derived hepatocytes. AASLD 2011.
5. Avsar Y, Zhou H, Wang X, Ding J, Guha C, Fox IJ, Roy-Chowdhury N, Roy-Chowdhury J. Pharmacological enhancement of hepatocyte engraftment augments the hypobilirubinemic effect of hepatocyte transplantation in the Gunn rat model of Crigler-Najjar syndrome type 1. AASLD 2011.
6. Ito R, Fong J, Setayama K, Gramignoli R, Tahan V, Nagaya M, Soto-Gutierrez A, Strom S, Fox IJ. Hepatocyte Xenografts Undergo Stable Long-Term Engraftment in Rats Treated with FK506 but Discordant Xenograft Albumin Secretion is 100-Fold Lower than Allograft Albumin Secretion. AST 2011.
7. Invited Speaker, iPS cell Banking Workshop, California Institute for Regenerative Medicine, San Francisco, CA, November 17-18, 2010.
8. Invited Speaker, Oregon Health and Science University Stem Cell Center, "Use of stem cells to study and treat liver disease" Portland, Oregon, February 7-8, 2011
9. Invited Speaker, AASLD Basic Research Single Topic Conference – Stem Cell in Liver Diseases and Cancer: Discovery and Promise, "Stem cells and the treatment of liver disease: understanding liver failure and cirrhosis, Atlanta, Georgia, March 19-20, 2011.
10. Invited Speaker, Yale University Stem Cell Center Seminar Series, "Stem cells and the liver" New Haven, Connecticut, March 28-29, 2011.
11. Invited Speaker, The 66th General Meeting of the Japanese Society of Gastroenterological Surgery, "Overcoming barriers to the use of hepatocytes and stem cells in treating patients with liver diseases", Nagoya, Japan, July 13-15, 2011.

CONCLUSIONS:

The outcomes of our studies are being accomplished as expected, and there is no change anticipated in the research plan. The intention for future studies is to attain better engraftment and more complete characterization of differentiated cells following transplantation.

REFERENCES

1. Basma H, Soto-Gutierrez A, Yannam GR, et al. Differentiation and transplantation of human embryonic stem cell-derived hepatocytes. Gastroenterology 2009;136:990-9.
2. Si-Tayeb K, Noto FK, Nagaoka M, et al. Highly efficient generation of human hepatocyte-like cells from induced pluripotent stem cells. Hepatology;51:297-305.

3. Roy-Chowdhury N, Chen Y, Atienza K, et al. Amelioration of hyperbilirubinemia in Gunn rats after transplantation of human hepatocytes derived from induced pluripotent stem cells. . AASLD 2010.
4. Overturf K, Al-Dhalimy M, Tanguay R, et al. Hepatocytes corrected by gene therapy are selected in vivo in a murine model of hereditary tyrosinaemia type I. Nat Genet 1996;12:266-73.
5. Rhim JA, Sandgren EP, Degen JL, Palmiter RD, Brinster RL. Replacement of diseased mouse liver by hepatic cell transplantation. Science 1994;263:1149-52.
6. Ding J, Yannam GR, Roy-Chowdhury N, et al. Spontaneous hepatic repopulation in transgenic mice expressing mutant human alpha1-antitrypsin by wild-type donor hepatocytes. The Journal of Clinical Investigation 2011;121:1930-4.
7. Ding J, Wang X, Neufeld DS, et al. SCID/PiZ mice: a novel animal model for evaluating engraftment and proliferation of human stem cell-derived hepatocytes. AASLD 2011.

NF-κB Negatively Impacts the Myogenic Potential of Muscle-Derived Stem Cells

Aiping Lu[1], Jonathan Proto[1], Lulin Guo[1], Ying Tang[1], Mitra Lavasani[1], Jeremy S. Tilstra[2], Laura J. Niedernhofer[2], Bing Wang[1], Denis C. Guttridge[3], Paul D. Robbins[2], and Johnny Huard[1] J.H. (jhuard@pitt.edu).

[1]Stem Cell Research Center, School of Medicine and Department of Orthopaedic Surgery, University of Pittsburgh, Pittsburgh, PA

[2]Department of Microbiology and Molecular Genetics, University of Pittsburgh, Pittsburgh, PA

[3]Department of Molecular Virology, Immunology and Medical Genetics, The Ohio State University, Columbus, OH

Correspondence: Johnny Huard, Ph.D., Stem Cell Research Center, 2 Bridgeside Point, 450 Technology Drive, Pittsburgh, PA 15219, USA. Telephone: 412-648-2789; Fax: 412-648-4066; e-mail: jhuard@pitt.edu

Running Title: NF-κB Suppresses Muscle Stem Cells function

ABSTRACT

Inhibition of the IKK/NF-κB pathway enhances muscle regeneration in injured and diseased skeletal muscle, but it is unclear exactly how this pathway contributes to the regeneration process. In this study, we examined the role of NF-κB in regulating the proliferation and differentiation of muscle-derived stem cells (MDSCs). MDSCs isolated from the skeletal muscles of *p65*$^{+/-}$ mice (haploinsufficient for the p65 subunit of NF-κB) had enhanced proliferation and differentiation compared to MDSCs isolated from wild-type (wt) littermates. In addition, selective pharmacological inhibition of IKKβ, an upstream activator of NF-κB, enhanced wt MDSC differentiation into myotubes *in vitro*. The *p65*$^{+/-}$ MDSCs also displayed a higher muscle regeneration index than wt MDSCs after their implantation into adult mice with muscular dystropy. Additionally, using a muscle injury model, we observed that p65$^{+/-}$ MDSC engraftments were associated with reduced inflammation and necrosis. These results suggest that inhibition of the IKK/NF-κB pathway represents an effective approach to improve the myogenic regenerative potential of MDSCs and possibly other adult stem cell populations. Moreover, our results suggest that the improved muscle regeneration observed following inhibition of IKK/NF-κB, is mediated, at least in part, through enhanced stem cell proliferation and myogenic potential.

INTRODUCTION

NF-κB is a ubiquitously expressed nuclear transcription factor that is evolutionarily conserved. In mammals, the NF-κB family consists of five subunits, p65 (RelA), c-Rel, RelB, p50 and p52 [1]. Transcriptionally active NF-κB exists as a dimer, with the most common form being a p50-p65 heterodimer. Under non-stress conditions, the heterodimer is maintained in an inactive state in the cytoplasm via its interaction with inhibitor of kappa B (IkB) proteins. Classic NF-κB activation is mediated by IkB kinase (IKK), a large, 700-900 kDa complex consisting of two catalytic subunits, IKKα and IKKß, and a regulatory subunit named IKKγ or NEMO (NF-κB essential modulator). In response to a variety of stimuli, including pro-inflammatory cytokines, bacterial products, viruses, growth factors, and oxidative stress, the complex is activated. Activated IKKß phosphorylates IkB, leading to its polyubiquitylation and subsequent degradation by the 26S proteasome. IkB degradation allows NF-κB to translocate to the nucleus where it binds to its cognate DNA site, as well as co-activators such as CBP/p300, to induce gene expression. Dysregulation of this pathway can result in chronic activation of IKK or NF-κB, and is seen in several pathophysiological states including cancer, rheumatoid arthritis, sepsis, muscular dystrophy, heart disease, inflammatory bowel disease, bone resorption, and both type I and II diabetes.

The NF-κB pathway, long recognized as an important component of innate and adaptive immunity, has also more recently emerged as al key player in the regulation of skeletal muscle homeostasis[2]. Furthermore, activation of NF-κB in skeletal muscle has been linked to cachexia, muscular dystrophies, and inflammatory myopathies [3-7]. Conversely, knock-out of p65, but not other subunits of NF-κB, enhances myogenic

activity in MyoD-expressing mouse embryonic fibroblasts (MEFs) [8]. Furthermore, genetic depletion of p65 enhances muscle regeneration in both mdx and wild-type murine skeletal muscle [7]. What remains unclear, however, is how reduction of NF-κB activity positively impacts muscle.

Given that the repair of damaged tissues is mediated by adult stem cell populations, we hypothesized that NF-κB activity negatively regulates muscle stem cell function. In this study, we specifically focus on the role of p65 in regulating muscle-derived stem cell (MDSC) growth and differentiation. This population of adult stem cells is capable of restoring muscle function [9, 10]. As complete knockout of p65 ($p65^{-/-}$) results in embryonic lethality, we isolated MDSCs from the skeletal muscles (SKM) of $p65^{+/-}$ mice and wt littermates [11]. We observed that, *in vitro*, p65 haploinsuffiency was associated with increased cell proliferation and myogenic differentiation. Pharmacologic inhibition of IKK/NF-κB also enhanced myogenic differentiation. We also demonstrated that $p65^{+/-}$ MDSCs have a higher capacity for muscle regeneration after implantation into dystrophic, mdx mouse SKM. Furthermore, we show that muscle inflammation and necrosis post-injury is decreased following $p65^{+/-}$ MDSC implantation into cardiotoxin injured SKM. These results suggest that reducing the activity of the IKK/NF-κB pathway is an effective approach to improve the myogenic potential of MDSCs and possibly other adult stem cell populations. Our results provide a novel mechanistic insight as to why the inhibition of this pathway promotes SKM healing.

RESULTS

Isolation and phenotypic characterization of MDSCs from $p65^{+/-}$ and wt mice. To examine the effect of NF-κB activity on MDSC function, we purified populations of

muscle stem cells from the SKM of mice heterozygous for the p65 subunit of NF-κB ($p65^{+/-}$) and wt littermates. Using a modified preplate technique [12], we isolated independent populations of MDSCs from three mice of each genotype. To confirm that p65 haploinsufficiency reduced basal levels of NF- κB activity, nuclear p65 was measured via ArrayScan^{Tm}. Nuclear, or active, p65 was found to be 30% lower in $p65^{+/-}$ than the wt MDSCs (**Fig. 1a**). Upon activation, NF-κB subunits undergo post-translational modifications, such as phosphorylation, to enhance their activity. Immunoblot analysis revealed that the level of phosphorylated p65 (P-p65) was also reduced; however, stimulation with TNFα led to an increased level of P-p65 in both wt and $p65^{+/-}$ MDSCs (**Fig. 1b**), demonstrating that basal, but not induced, NF-κB activity is affected by knocking-out one allele of *p65*.

To confirm the MDSC phenotype of $p65^{+/-}$ and wt cells, each population was analyzed for the expression of stem (CD34, Sca-1), myogenic (MyoD and desmin), and endothelial (CD144, CD31) cell markers by RT-PCR. For each of the markers, there was variability in expression between cell populations of a single genotype, but upon quantification, no significant differences were found between the different genotypes, with the exception of CD144, which was elevated in $p65^{+/-}$ MDSCs. (**Figs. 2a,c, $p<0.05$**). Such variability in marker expression has been previously reported and interpreted as evidence that these cell populations contain a mix of stem and committed progenitor cells [13], [14]. We next examined the expression Pax7 and MyoD protein by immmunostaining, and also found no significant difference between $p65^{+/-}$ and wt cells (**Figs. 2b,d**). These results suggest that genetic reduction of p65 does not dramatically alter the phenotype of MDSCs.

p65$^{+/-}$ MDSCs proliferate faster than* wt *MDSCs. NF-κB is known to regulate cell division, so we investigated whether p65 reduction would alter MDSC proliferation. The 3 populations of *p65*$^{+/-}$ and wt MDSCs were plated in collagen-coated flasks and expanded in growth medium for 10 to 12 passages. Cells were then transferred to 24 well plates and proliferation measured using a previously described Live Cell Imaging (LCI) system [15]. We observed that *p65*$^{+/-}$ MDSCs proliferated significantly faster than wt cells (**Fig. 3a, Supplemental movie 1-2**). Equal numbers of cells were also plated on a 96 well plate and grown for three days at which point the differences in cell number were determined using an MTS assay. This assay demonstrated a similar significant increase in cell proliferation in *p65*$^{+/-}$ MDSCs (**Fig. 3b**) suggesting that NF-κB, and in particular p65, limits the proliferation of MDSCs.

p65$^{+/-}$ MDSCs have enhanced myogenic differentiation compared to wt cells. We next measured the ability of the *p65*$^{+/-}$ and wt MDSCs to undergo myogenic differentiation *in vitro*. Equal numbers of cells were plated in a 24 well plate and switched to differentiation medium once the cells adhered. After 3 days the majority (80%) of the *p65*$^{+/-}$ cells had differentiated into myotubes, as determined by immunodetection of myosin heavy chain (**Fig. 4a**). The differentiation potential of the *p65*$^{+/-}$ MDSCs was significantly greater than the wt MDSCs (60%; $p<0.01$; **Fig. 4b)** The difference was also demonstrated using the LCI system described above (**Supplemental movie 3-4)**. These results demonstrate that NF-κB, and in particular p65, represses MDSC differentiation *in vitro*.

Pharmacologic inhibition of IKKβ increases myogenic differentiation in vitro. To confirm this finding implicating NF-kB as negatively impacting MDSC differentiation,

we tested whether a pharmacologic inhibitor of NF-κB could enhance MDSC myogenic potential *in vitro*. Wt MDSCs were exposed to differentiation medium containing various doses of the IKK-2 inhibitor IV (IKKi), a specific, reversible inhibitor of IKKß. Cell lysates were collected at 0, 1, 14, 24, 48, and 72 hrs following treatment. Accordingly, MyHC levels dramatically increased, beginning at 14 hrs (**Figs. 5a,c**). As expected, we observed a robust time-dependent decrease in P-p65 that was dose-dependent (greater at 3 μM than 1 μM; **Fig. 5b)**. We next examined NF-κB activity in wt and $p65^{+/-}$ MDSCs at various time points during myogenic differentiation by immunodetection of P-p65 and MyHC. In wt cells, beginning at 48 hrs post-transition to differentiation medium, the levels of p-p65 were detectably reduced (**Fig. 5d**). This occurred more rapidly (by 24 hrs) in $p65^{+/-}$ cells. Similarly, accumulation of MyHC was greater at earlier time points (14 hrs) in $p65^{+/-}$ cells than wt. This timeframe for MyHC accumulation is similar to that observed in wt cells treated with IKKi (**Fig. 5a**). In order to verify that increased MyHC expression was concomitant with increased myotube formation, we treated wt MDSCs with 5 μM IKKi. After three days, differentiation was assessed by immunofluorescence detection of MyHC. As shown in **Fig. 5e,** compared to non-treated controls, the inhibitor caused a significant increase in myotube formation. The level of myogenic differentiation was comparable to that of $p65^{+/-}$ MDSCs ($p<0.01$; **Fig. 5f**). These results provide strong support that MDSC myogenic potential can be improved using NF-κB inhibition *ex vivo*.

$p65^{+/-}$ MDSCs have greater muscle regenerative capacity in vivo. To determine if genetic depletion of p65 increases the engraftment and muscle regenerative capacity of MDSCs *in vivo*, we examined the ability of $p65^{+/-}$ and wt MDSCs to regenerate muscle fibers following their intramuscular implantation into an immunocompromised model of

Duchenne Muscular Dystrophy. For these experiments, $3x10^5$ *p65*$^{+/-}$ and wt MDSCs were injected into the gastrocnemius muscles of 8 wk-old dystrophin-deficient SCID (mdx/SCID) mice. Fourteen days post-implantation, significantly more dystrophin-positive myofibers were detected in the muscle injected with *p65*$^{+/-}$ MDSCs than in muscle injected with wt MDSCs ($p<0.01$; **Figs. 6a,b**). These results confirm our *in vitro* observations and may provide a novel mechanism as to why IKK inhibitors have been reported to improve muscle regeneration [16].

Transplantation of p65$^{+/-}$ MDSCs post-injury reduces SKM inflammation and necrosis. The results above suggest that lowering basal levels of NF-κB activity increased the ability of MDSCs to engraft and differentiate following intramuscular injection (**Fig 6**). However, while it is possible this is mediated through enhanced proliferation and differentiation, the exact mechanism as to why more dystrophin-positive myofibers were found within the *p65*$^{+/-}$ MDSC engraftment sites remains unclear. Surrounding the engraftments of the wt MDSCs, we observed numerous cells positive for the macrophage marker CD14 as detected by immunofluorescent staining (data not shown), whereas the *p65*$^{+/-}$ MDSC engraftment sites were surrounded by fewer numbers of CD14+ cells (data not shown). As the mdx/SCID is an immunocompromised mouse model with a high level of background inflammation, we decided to further investigate this phenomenon using the well established cardiotoxin (CTX) muscle injury model in immunocompetent wild type mice. In order to confirm that transplanted *p65*$^{+/-}$ MDSCs are able to reduce inflammation in host skeletal muscle, we injected *p65*$^{+/-}$ and wt MDSCs into the gastrocnemius muscles of 8 wk-old C57BL/6J mice 24 hours post-CTX injury. Six days post-transplantation, the wt MDSC engraftment area demonstrated a

greater number of inflammatory cells surrounding the wt donor MDSCs than the *p65*$^{+/-}$ MDSCs. Furthermore, numerous centrally located nuclei, characteristic of regenerating muscle fibers, were found within the *p65*$^{+/-}$ MDSC injection sites. Consistent with observations made in mdx/SCID mice, the *p65*$^{+/-}$ MDSC engraftment area was associated with significantly fewer CD14 positive cells than the wt MDSC engraftment area ($p<0.01$**; Figs.7a, b**). There was also a significant (42%) reduction in tissue necrosis, as determined by quantification of mouse IgG staining (**p**<0.01; **Figs.7a, c**). These results indicate that the improved engraftment and differentiation of *p65*$^{+/-}$ MDSCs is potentially due to their ability to attenuate the inflammation and necrosis that typically occurs after muscle injury.

DISCUSSION

NF-κB signaling has been implicated in the regulation of muscle degeneration and regeneration. The five mammalian NF-κB transcription factors are all expressed in skeletal muscle to modulate a variety of processes, including apoptosis, inflammation, and myoblast differentiation. Although there have been conflicting results reported as to whether NF-κB acts as a repressor or promoter of myogenesis [2, 17-22], recent results suggest that the classical NF-κB signaling pathway functions as a negative regulator of myogenesis [8]. In addition, NF-κB activation is associated with the degeneration and/or lack of regeneration of dystrophic muscle in mdx mice [7]. Thus, in this study, we examined the effect of NF-κB reduction on the proliferation and differentiation of MDSCs isolated from wt mice and mice heterozygous for p65. Although *p65*$^{+/-}$ MDSCs had a more than a 30% reduction in p65/NF-kB levels compared to the wt MDSCs, the two genotypes expressed similar stem (CD34, Sca-1), myogenic (Desmin, MyoD) and

endothelial (CD144, CD31) cell markers. This result suggests that the reduction in NF-kB did not affect overall expression of MDSCs markers, albeit there is some variability in stem cell marker expression between populations of the same genotype.

We observed that MDSCs with reduced p65 levels have improved proliferation compared to wt control cells, suggesting that p65/NF-κB activity negatively controls MDSC expansion. More importantly, we also observed that both the rate and extent of myogenic differentiation was accelerated in MDSCs with reduced p65 and in wt MDSCs treated with an IKKß inhibitor. Together, these data suggest that NF-κB inhibits muscle stem cell differentiation. Our results are in agreement with previous studies showing that regulation of myogenesis is dependent on p65 transcriptional activity, which is able to inhibit myogenesis [8]. It has been suggested previously that the negative effect of NF-κB on differentiation is mediated through the transcriptional activation of cyclin D1 and YinYang1 (YY1) [23, 24]. Interestingly, we have observed a reduction in the level of cyclin D1 in $p65^{+/-}$ MDSCs compared to wt cells, but found no difference in the level of YY1 expression (data not shown).

Recent genetic evidence supports the role of IKK/NF-κB in driving the pathogenesis of muscular dystrophy, identifying this signaling pathway a potential therapeutic target for the treatment of DMD [7]. The activity of NF-κB in dystrophic muscle is associated with not only immune cells, but also regenerative muscle fibers. Thus we investigated whether the $p65^{+/-}$ MDSCs have a higher muscle regeneration potential than wt MDSCs after their intramuscular injection into dystrophic mdx/SCID skeletal muscles. Our results demonstrated that $p65^{+/-}$ MDSCs are more efficient at regenerating dystrophin positive

myofibers compared to wt MDSCs, which is consistent with the enhanced ability of the *p65*$^{+/-}$ MDSCs to differentiate in culture.

We also assessed inflammation around the engrafted site by immunofluorescent staining for CD14, a macrophage marker. While we found very few CD14 positive cells within the injection sites of the *p65*$^{+/-}$ cells, many CD14+ cells were detected within the wt MDSC engraftment areas. As decreased macrophage invasion in the *p65*$^{+/-}$ cell engraftment area correlated with a reduction in necrosis, it is possible that a reduction in p65 enhances the local anti-inflammatory properties of MDSCs via regulation of paracrine factors. Several cytokines under control of NF-κB, such as tumor necrosis factor alpha (TNFα) and IL-6, are potent inhibitors of myogenic differentiation [2]. Thus, taken together, these results suggest that inhibition of NF-κB/p65 may enhance myogenesis by reducing inflammation and necrosis.

Other groups have demonstrated the importance of non-NF-kB proteins in muscle development and pathology. During regeneration following injury, numerous paracrine factors such as myostatin, hepatocyte growth factor (HGF), and basic fibroblast growth factor play critical roles coordinating repair[25]. For example, myostatin acts independently of the classical TNFα and NF-kB pathway to inhibit MyoD expression and signal cachexia by reversing the IGF-1/PI3K/AKT hypertrophy pathway to increase the levels of active FoxO1, allowing for increased expression of atrophy-related genes[26]. **In summary**, here we described a negative role for the p65/NF-κB signaling pathway in MDSC growth and differentiation *in vitro*, as well as muscle regeneration *in vivo*. Similarly, pharmacological inhibition of IKKβ identifies the IKK/NF-κB signaling

pathway as a potential therapeutic target to improve the myogenic potential of MDSCs and muscle regeneration after injury and diseases.

MATERIALS AND METHODS

Animals: The C57BL/6J mice heterozygous for p65/RelA were originally described by Amer Beg[11]. The mdx/SCID (C57BL/10ScSn DMD^{mdx}/J/CB17-Prkdc^{scid}/J) and C57BL/6J mice were obtained from the Jackson Laboratory (Bar Harbor, ME). All animal protocols used for these experiments were approved by the Children's Hospital of Pittsburgh's Institutional Animal Care and Use Committee.

Isolation of MDSCs from p65$^{+/-}$ mice. The mice were sacrificed at 5 months of age and muscle stem cell isolation was performed as previously described via a modified preplate technique [12]. Briefly, the SKM tissue was minced and processed through a series of enzymatic dissociations: 0.2% of collagenase type XI (Sigma-Aldrich, St. Louis, MO) for 1 hr, 2.4 units/ml of dispase (Invitrogen, Carlsbad, CA) for 45 min, and 0.1% of trypsin-EDTA (Invitrogen) for 30 min at 37^{o}C. After enzymatic dissociation, the muscle cells were centrifuged and re-suspended in proliferation medium (DMEM supplemented with 10% FBS, 10% HS, 0.5% chicken embryo extract, and 1% Penicillin-streptomycin), and the resulting cell suspension from both *p65*$^{+/-}$ and wt muscle were plated in collagen type I coated flasks. Different populations of muscle-derived cells were isolated based on their adhesion characteristics. After 7 days, late preplate populations (slow adhering cells) were obtained and cultured in proliferation medium. The slowly adhering fraction of muscle cells has been previously shown to contain MDSCs [12]. For all experiments, congenic *p65*$^{+/-}$ and *p65*$^{+/+}$ MDSCs of the same passage number were compared.

p65 staining and ArrayScan Assay. Cells were fixed with 4% paraformaldehyde for 15 min at room temperature (RT), rinsed 2 times with PBS, and the cells' membrane permeabilized for 10 min with 0.1% Triton X-100 in PBS. A 10% goat serum blocking solution was used for 1 hr and the cells were incubated with a 1:200 dilution of rabbit polyclonal anti-p65 (Abcam, Cambridge, MA) for 1 hr at RT. After washing 3 times, the cells were incubated for 30 min with Cy3-conjugated anti-rabbit IgG (1:500, Sigma-Aldrich). The nuclei were revealed by 4', 6-Diamidino-2-phenylindole (DAPI) staining. Nuclear localization of the NF-κB subunit p65 was measured via ArrayScan^{Tm}. This technique allows for the rapid, automated quantification of p65 and DAPI colocalization, as identified by immunocytochemistry in cells grown on a 96-well plate. Recordings were taken from multiple fields of view per well, generating data representative of each well.

Western Blot assay. The cell populations isolated from *p65*$^{+/-}$ and wt mice were cultured in proliferation medium and stimulated with TNFα (10 ng/ml) for 30 min prior to harvesting. Cells were then lysed in Laemmli Sample Buffer (Bio-Rad, Hercules, CA), boiled for 5 min, and centrifuged at 4000 rpm for 5 min. Each sample was loaded on a 10% SDS-polyacrylamide gel, which was run for 2 hrs and then transferred for 1.5 hrs at 100 volts while stirring on ice. The membrane was blocked with 5% bovine serum albumin (Sigma) in PBS for 1 hr and then incubated with rabbit anti-phospho-NF-κB/p65 monoclonal antibody (1:1000, Cell signaling, Danvers, MA) overnight at 4°C. After washing 3 times with Tris-buffered saline tween-20 (TBST), the membrane was incubated with goat anti-rabbit IgG (H+L) (1:5000, Pierce, Rockford, IL) for 50 min at room temperature (RT). Blots were developed by ECL solution (Pierce).

RT-PCR analysis. Total RNA was extracted from cells using Nucleo Spin RNA II column (Clontech, Mountain View, CA). Following isolation, cDNA was synthesized with SuperScript^{TM} II reverse transcriptase (Invitrogen), according to the manufacturer's instructions. PCR was performed with Taq polymerase (Invitrogen) as per the manufacturer's instructions and PCR products were separated by electrophoresis with 1% agarose gels. The primers used for PCR are listed in Table 1. Each set of oligonucleotides was designed to span two different exons to avoid background amplification of genomic DNA. The data were quantified by densitometry using Adobe Photoshop 7.0.

Pax7 and MyoD staining. *P65*$^{+/-}$ and wt cells were fixed and permeabilized with 2% paraformaldehyde plus 1% Triton X-100 for 30 min at 4°C and rinsed 2 times with PBS. Cells were blocked with 5% HS and then incubated with a 1:100 dilution of mouse monoclonal anti-Pax7 (DSHB, Iowa City, Iowa) and anti-MyoD (Santa Cruz biotechnology, Santa Cruz, CA) over night at 4°C. After washing 3 times, the cells were incubated for one hour with biotinylated anti-mouse IgG (1:300, Vector Lab, Burlingame, CA), which acted as a secondary antibody. Streptavidin 594 conjugate (1:500, Invitrogen) was added in the last step. The nuclei were revealed by DAPI staining. Negative control staining was performed by an identical procedure, with the exception that the primary antibody was omitted.

In vitro Assessment of Cell Proliferation. In order to compare the proliferative potential of *p65*$^{+/-}$ MDSCs to wt MDSCs, we used a previously described live cell imaging system [LCI] (Kairos Instruments LLC) [15]. Brightfield images were taken at a 100x magnification at ten min intervals over a 72 hour period in three fields of view per well, with three wells per population. The images were combined to generate a movie

using ImageJ software (NIH). Proliferation was assessed by counting the number of cells per field of view, n, over twelve hours. All six populations were also plated in 96-well plates in quadruplicate (500 cells/well) and cultured under normal conditions for 72 hours. At this time, 20 uL of CellTiter96 AQueous One Reagent (Promega, Madison, WI) was added to each well and incubated in 5% CO_2 at 37 °C. Following another 3 hour incubation, absorbance at 490 nm was read with a 96-well plate reader.

Myogenic differentiation assay and fast Myosin Heavy Chain (MyHC-f) staining. After 15 passages, cells were plated on 12 well plates (30,000 cells per well) with DMEM supplemented with 2% FBS to stimulate myotube formation. Three days later, immunocytochemical staining for fast skeletal Myosin Heavy Chain (MyHC-f) was performed. After rinsing 3 times with PBS, cells were fixed for 2 min in cold methanol, blocked with 10% horse serum for one hr and then incubated with a mouse anti-MyHC-f (1:250, Sigma, clone MY-32) for 2 hr at RT. The primary antibody was detected with a secondary anti-mouse IgG antibody conjugated with Cy3 (1:300, Sigma) for 15 min. The nuclei were revealed by DAPI staining. The percentage of differentiated myotubes was quantified as the number of nuclei in MyHC-f positive myotubes relative to the total number of nuclei. The myogenic differentiation was also monitored over a period of 5 days using Live Cell Imaging. The images were combined to create a movie using ImageJ software (NIH).

Selective Inhibition of IKKβ. To determine the effects of IKK/NF-κB inhibition on wt MDSCs during myogenic differentiation, we utilized IKK-2 Inhibitor IV(IKKi), or 2-[(Aminocarbonyl)amino]-5-(4-fluorophenyl)-3-thiophenecarboxamide (Calbiochem, San Diego, CA), a reversible competitive inhibitor of IKKβ ATP binding. Cells were

plated at 10^5 cells per well in 6 well plates and exposed to IKK inhibitor in differentiation medium. Cells were treated with either 1, 3, or 5 uM IKKi. Lysates were collected at 0 min, 14, 24, 48, and 72 hrs following treatment. NF-kB activity and myogenic differentation was assessed by western blot for phosphorylated NF-kB/p65 (1:1000, Cell signaling, Danvers, MA) and MyHC-f (1:500, Sigma, clone MY-32), as detailed above.

Cell implantation and Dystrophin staining. MDSCs from *p65*$^{+/-}$ and wt muscle were grown in proliferation medium until the cell number was sufficient for injection. A total of 3x10^5 viable cells was suspended in 20 µl of Hank's balanced salts solution (HBSS) and injected into the gastrocnemius muscles of 8-12 wk-old mdx/SCID mice using a Hamilton syringe. The same number of cells was injected into the gastrocnemius muscles of 8 wk-old wt C57BL/6J mice that had been injured 1 day earlier by a 30 µL intramuscular injection of 2µM cardiotoxin (CTX; Sigma) in PBS. The cell suspension was mixed with green fluorescent-labeled beads prior to injection to detect the injection sites. Six or fourteen days after implantation, the mice were sacrificed and the gastrocnemius muscles were harvested and flash frozen in liquid nitrogen-cooled 2-methylbutane. Serial cryosections 10 µm in thickness were obtained for immunohistochemical analyses. Cryosections were fixed with 5% formalin and blocked with 5% donkey serum in PBS for 1 h, then incubated with rabbit anti-dystrophin (1:300, Abcam) for 2 hr at RT. The sections were exposed to secondary 594-conjugated anti-rabbit IgG (1:500, Invitrogen) in PBS for 30 min. The nuclei were revealed by DAPI staining. Immunostaining was visualized and images were taken by fluorescence microscopy (Nikon Eclipse E800). Northern Eclipse software was used for quantitative analysis of the regenerated dystrophin-positive myofibers. A series of pictures were

taken, and Adobe Photoshop 7.0 was used to construct a composite picture of the dystrophin-positive myofibers, which were then manually counted.

Retroviral transduction of MDSCs . MDSCs were plated at an initial confluence of 30-40% and retrovirally transduced (in the presence of Polybrene[8 μg/ml]) to express the beta-galactosidase gene (LacZ), as previously described[27].

LacZ staining The cryosections were fixed in 1% glutaraldehyde and incubated 3 hours with 5-bromo-4-chloro-3-indolyl b-D-galactopyranoside (X-gal) substrate at room temperature (RT). Sections were counterstained with Eosin.

CD14 staining. Cryosections were fixed with 5% formalin and blocked with 5% donkey serum in PBS for 1 h, then incubated with rat anti-CD14 (1:200, Biolegend, San Diego, CA) overnight at 4ºC. This was followed by a 1 hr incubation with biotinylated anti-rat IgG (1:300, Vector). Streptavidin Cy3 conjugate (1:500, Sigma) was added in the last step followed by several rinses in PBS. Following CD14 staining, five random pictures per section were taken and the number of CD14 positive cells was counted manually.

Mouse IgG staining and quantification of necrosis. Muscle sections were fixed with 5% formalin and blocked with 10% horse serum in PBS for 1 hr, then incubated with biotinylated anti mouse IgG (1:300; Vector) for 1 hr at RT. This was followed by a 15 min incubation with streptavidin Cy3 conjugate (1:500, Sigma). The nuclei were revealed by DAPI staining. The IgG positive area was measured and quantified as the percentage of mouse IgG expressing area per total area using Northern Eclipse software.

Statistical analysis. All results are given as the mean ± standard deviation. Means from $p65^{+/-}$ and wt or treated and untreated were compared using Students' *t*-test. Differences were considered statistically significant when the p-value was <0.05.

ACKNOWLEDGEMENT

The authors thank the members of the Huard laboratory, especially Jenny Zhu and Bin Sun for discussions and technical advice. Special thanks go to Joseph Feduska and Bridget Deasy for live cell imaging advice. This work was supported in part by the Henry J. Mankin Endowed Chair for Orthopaedic Research at the University of Pittsburgh, the William F. and Jean W. Donaldson Chair at Children's Hospital of Pittsburgh. L.J.N. is supported by NIEHS (ES016114) and NIA (AG033907).

The authors do not have conflicts of interest to disclose other than the corresponding author who receives consulting fees from Cook MyoSite Inc.

SUPPLEMENTARY MATERIAL

Supplemental movie 1. $P65^{+/-}$ MDSCs proliferation

Supplemental movie 2. wt MDSCs proliferation

Supplemental movie 3. $P65^{+/-}$ MDSCs differentiation

Supplemental movie 4. wt MDSCs differentiation

SUPPLEMENTAL MOVIE LEGEND

Movie 1. MDSCs isolated from $p65^{+/-}$ mouse SKM have a higher rate of proliferation than wt cells. The $p65^{+/-}$ cell proliferation rate was measured by Live cell imaging.

Brightfield images were taken at a 100x magnification at ten min intervals over a 72 hour period.

Movie 2. MDSCs isolated from wt mouse SKM have a lower rate of proliferation than *p65*$^{+/-}$ cells. The wt cell proliferation rate was measured by Live cell imaging. Brightfield images were taken at a 100x magnification at ten min intervals over a 72 hour period.

Movie 3. Myogenic differentiation is enhanced in MDSCs isolated from *p65*$^{+/-}$ mouse SKM compared to wt MDSCs *in vitro*. The *p65*$^{+/-}$ cell differentiation was monitored over a period of 5 days using Live Cell Imaging.

Movie 4. The wt cell differentiation was also monitored over a period of 5 days using Live Cell Imaging. Less myotube formation was found in this wt MDSCs compared to *p65*$^{+/-}$ MDSCs.

REFERENCES

1. Verma IM, Stevenson JK, Schwarz EM, Van Antwerp D, Miyamoto S. Rel/NF-kappa B/I kappa B family: intimate tales of association and dissociation. *Genes Dev* 1995; **9**(22)**:** 2723-35.

2. Langen RC, Schols AM, Kelders MC, Wouters EF, Janssen-Heininger YM. Inflammatory cytokines inhibit myogenic differentiation through activation of nuclear factor-kappaB. *FASEB J* 2001; **15**(7)**:** 1169-80.

3. Baghdiguian S, Martin M, Richard I, Pons F, Astier C, Bourg N *et al.* Calpain 3 deficiency is associated with myonuclear apoptosis and profound perturbation of the IkappaB alpha/NF-kappaB pathway in limb-girdle muscular dystrophy type 2A. *Nat Med* 1999; **5**(5)**:** 503-11.

4. Kumar A, Lnu S, Malya R, Barron D, Moore J, Corry DB *et al.* Mechanical stretch activates nuclear factor-kappaB, activator protein-1, and mitogen-activated protein kinases in lung parenchyma: implications in asthma. *Faseb J* 2003; **17**(13)**:** 1800-11.

5. Monici MC, Aguennouz M, Mazzeo A, Messina C, Vita G. Activation of nuclear factor-kappaB in inflammatory myopathies and Duchenne muscular dystrophy. *Neurology* 2003; **60**(6)**:** 993-7.

6. Hunter RB, Kandarian SC. Disruption of either the Nfkb1 or the Bcl3 gene inhibits skeletal muscle atrophy. *J Clin Invest* 2004; **114**(10)**:** 1504-11.

7. Acharyya S, Villalta SA, Bakkar N, Bupha-Intr T, Janssen PM, Carathers M *et al.* Interplay of IKK/NF-kappaB signaling in macrophages and myofibers promotes muscle degeneration in Duchenne muscular dystrophy. *J Clin Invest* 2007; **117**(4)**:** 889-901.

8. Bakkar N, Wang J, Ladner KJ, Wang H, Dahlman JM, Carathers M *et al.* IKK/NF-kappaB regulates skeletal myogenesis via a signaling switch to inhibit differentiation and promote mitochondrial biogenesis. *J Cell Biol* 2008; **180**(4)**:** 787-802.

9. Payne TR, Oshima H, Okada M, Momoi N, Tobita K, Keller BB *et al.* A relationship between vascular endothelial growth factor, angiogenesis, and cardiac repair after muscle stem cell transplantation into ischemic hearts. *J Am Coll Cardiol* 2007; **50**(17)**:** 1677-84.

10. Ambrosio F, Ferrari RJ, Distefano G, Plassmeyer JM, Carvell GE, Deasy BM *et al.* The synergistic effect of treadmill running on stem-cell transplantation to heal injured skeletal muscle. *Tissue Eng Part A* 2010; **16**(3)**:** 839-49.

11. Beg AA, Sha WC, Bronson RT, Ghosh S, Baltimore D. Embryonic lethality and liver degeneration in mice lacking the RelA component of NF-kappa B. *Nature* 1995; **376**(6536)**:** 167-70.

12. Gharaibeh B, Lu A, Tebbets J, Zheng B, Feduska J, Crisan M *et al.* Isolation of a slowly adhering cell fraction containing stem cells from murine skeletal muscle by the preplate technique. *Nat Protoc* 2008; **3**(9)**:** 1501-9.

13. Sacco A, Doyonnas R, Kraft P, Vitorovic S, Blau HM. Self-renewal and expansion of single transplanted muscle stem cells. *Nature* 2008; **456**(7221)**:** 502-6.

14. Jankowski RJ, Haluszczak C, Trucco M, Huard J. Flow cytometric characterization of myogenic cell populations obtained via the preplate technique: potential for rapid isolation of muscle-derived stem cells. *Hum Gene Ther* 2001; **12**(6)**:** 619-28.

15. Deasy BM, Jankowski RJ, Payne TR, Cao B, Goff JP, Greenberger JS *et al.* Modeling stem cell population growth: incorporating terms for proliferative heterogeneity. *Stem Cells* 2003; **21**(5)**:** 536-45.

16. Tang Y, Reay DP, Salay MN, Mi MY, Clemens PR, Guttridge DC *et al.* Inhibition of the IKK/NF-kappaB pathway by AAV gene transfer improves muscle regeneration in older mdx mice. *Gene Ther* 2010.

17. Lehtinen SK, Rahkila P, Helenius M, Korhonen P, Salminen A. Down-regulation of transcription factors AP-1, Sp-1, and NF-kappa B precedes myocyte differentiation. *Biochem Biophys Res Commun* 1996; **229**(1)**:** 36-43.

18. Guttridge DC, Albanese C, Reuther JY, Pestell RG, Baldwin AS, Jr. NF-kappaB controls cell growth and differentiation through transcriptional regulation of cyclin D1. *Mol Cell Biol* 1999; **19**(8)**:** 5785-99.

19. Kaliman PA, Barannik TV. Regulation of delta-aminolevulinate synthase activity during the development of oxidative stress. *Biochemistry (Mosc)* 1999; **64**(6)**:** 699-704.

20. Canicio J, Ruiz-Lozano P, Carrasco M, Palacin M, Chien K, Zorzano A *et al.* Nuclear factor kappa B-inducing kinase and Ikappa B kinase-alpha signal skeletal muscle cell differentiation. *J Biol Chem* 2001; **276**(23)**:** 20228-33.

21. Munz B, Hildt E, Springer ML, Blau HM. RIP2, a checkpoint in myogenic differentiation. *Mol Cell Biol* 2002; **22**(16)**:** 5879-86.

22. Baeza-Raja B, Munoz-Canoves P. p38 MAPK-induced nuclear factor-kappaB activity is required for skeletal muscle differentiation: role of interleukin-6. *Mol Biol Cell* 2004; **15**(4)**:** 2013-26.

23. Guttridge DC, Mayo MW, Madrid LV, Wang CY, Baldwin AS, Jr. NF-kappaB-induced loss of MyoD messenger RNA: possible role in muscle decay and cachexia. *Science* 2000; **289**(5488)**:** 2363-6.

24. Wang H, Hertlein E, Bakkar N, Sun H, Acharyya S, Wang J *et al.* NF-kappaB regulation of YY1 inhibits skeletal myogenesis through transcriptional silencing of myofibrillar genes. *Mol Cell Biol* 2007; **27**(12)**:** 4374-87.

25. Karalaki M, Fili S, Philippou A, Koutsilieris M. Muscle regeneration: cellular and molecular events. *In Vivo* 2009; **23**(5)**:** 779-96.

26. McFarlane C, Plummer E, Thomas M, Hennebry A, Ashby M, Ling N *et al.* Myostatin induces cachexia by activating the ubiquitin proteolytic system through an NF-kappaB-independent, FoxO1-dependent mechanism. *J Cell Physiol* 2006; **209**(2)**:** 501-14.

27. Li Y, Huard J. Differentiation of muscle-derived cells into myofibroblasts in injured skeletal muscle. *Am J Pathol* 2002; **161**(3)**:** 895-907.

Table 1 Primers used for RT–PCR

Gene	Forward primer	Reverse primer	Location
Sca-1	CCTACTGTGTGCAGAAAGAGC	CAGGAAGTCTTCACGTTGACC	89–331
CD34	GCAGCTTTGAGATGACATCACC	CTCAGCCTCCTCCTTTTCACA	498–715
MyoD1	ACAGTGGCGACTCAGATGCATC	GCTGCAGTCGATCTCTCAAAGC	708–1105
Desmin	AACCTGATAGACGACCTGCAG	GCTTGGACATGTCCATCTCCA	615–873
CD31	AGAGCTACGTCATTCCTCAG	GACCAAGTGTGTCACTTGAAC	474–988
CD144	CACCAACAAAAACCTGGAACA	CCACCACGATCTTGTATTCAG	425–729
β-Actin	TCAGAAGGACTCCTATGTGG	TCTTTGATGTCACGCACGAT	234–722

FIGURE LEGENDS

Figure 1. MDSCs obtained from the SKM of *p65*$^{+/-}$ mice have a lower level of activated p65 compared to wt MDSCs (**a**) ArrayScan^{Tm} analysis of nuclear p65 in MDSCs isolated from *p65*$^{+/-}$ and wt mice. Error bars indicate "mean + SD". **(b)** Immunoblotting for phosphorylated p65 in whole cell lysates of MDSCs before and after TNFα stimulation for 30 minutes.

Figure 2. *p65*$^{+/-}$ and wt MDSCs exhibit a similar molecular marker profile. (**a**) RNA was isolated from three independent cell populations of each genotype. RT-PCR was performed to characterize the MDSC populations for the expression of stem (CD34 and Sca-1), endothelial (CD31 and CD 144) and myogenic (MyoD and desmin) cell markers. (**b**) Immunostaining for the muscle stem cell markers Pax7 and MyoD was also performed (scale bar=25 μm). (**c**) Quantification of RT-PCR results. Error bars indicate "mean + SD". (n=3 independent experiments). (**d**) Quantification of Immunostaining of Pax7 and MyoD.

Figure 3. MDSCs isolated from *p65*$^{+/-}$ mouse SKM have a higher rate of proliferation than wt cells. (**a**) Cell proliferation rate was measured by Live cell imaging and (**b**) by an MTS assay ($p<0.05$).

Figure 4. Myogenic differentiation is enhanced in MDSCs isolated from *p65*$^{+/-}$ mouse SKM compared to wt MDSCs *in vitro*. (**a**) MDSCs were cultured in myogenic differentiation medium for 3 days, during which cell fusion into multinucleated myotubes

was monitored using bright field microscopy and then confirmed by immunostaining for MyHC. (**b**) Quantitation of MyHC positive myotubes. The percentage of differentiated myotubes was quantified as the number of nuclei in MyHC-f positive myotubes relative to the total number of nuclei. A total of 3 populations of *p65*$^{+/-}$ and wt MDSCs were tested ($p<0.05$). In panel "**a**" all bars=200μm on bright field and all bars=50μm on MyHC immunostaining.

Figure 5. MDSC myogenic differentiation is enhanced by pharmacological inhibition of IKKβ. (**a**) Western blot for MyHC over 72 hrs of wt MDSCs treated with 1, 3, or 5 uM IKKi during differentiation. (**b**) Western blot for P-p65 over 72 hrs of wt MDSCs treated with 1, 3, or 5 uM IKKi during differentiation. (**c**) Quantification of **b**, MyHC levels during differentiation (n=3 independent experiments). **(d)** In parallel, wt and *p65*$^{+/-}$ MDSCs were cultured in differentiation medium and lysates were collected at the various time points indicated. Lysates were used for western blot for MyHC and P-p65 levels. (**e**) In parallel, wt MDSCs, *p65*$^{+/-}$ MDSCs, and wt MDSCs treated with IKKi (5uM), were grown under fusion conditons for 72 hrs and immunostained for MyHC expression (**f**) Quantification of MyHC staining ($p<0.05$). In panel "**e**" all bars=100μm.

Figure 6. Heterozygous deletion of p65 promotes the regeneration capacity of MDSCs. (**a**) Gastrocnemius cryosections from 8 wk-old mdx/SCID mice in which *p65*$^{+/-}$ and wt MDSCs were implanted. Engraftment was determined by immunostaining for dystrophin (red). Three populations of *p65*$^{+/-}$ and wt MDSCs were transplanted into 12 mice in two

independent experiments. (**b**) Quantitation of regenerated dystrophin-positive myofibers ($p<0.05$). In panel "**a**" all bars=50μm. Error bars indicate "mean + SD" (n=9).

Figure 7. *p65*$^{+/-}$ MDSCs attenuate muscle inflammation and necrosis. (**a**) Gastrocnemius cryosections from 8 wk-old C57BL/6J mice, which were injected with *p65*$^{+/-}$ or wt MDSCs 24 hours post-CTX injury. LacZ and Eosin staining identified the injection area and immunostaining for CD14 (red) and mouse IgG (red) identified macrophages and necrotic tissue, respectively. In immunological stains, fluorescent green beads in C57BL/6J muscle sections confirmed the location of injection sites. (**b**) Quantitation of CD14 positive cells (the data represent 6 muscles per group). (**c**) Necrotic area in the gastrocnemius muscles was identified by IgG staining and quantitated based on the total positive area per image (the data represent 6 muscles per group). In panel "**a**" all bars=100μm on LacZ+Eosin and mouse IgG staining. All bars=50μm on CD14 staining.

Transplantation of p65 Deficient Stem Cells Improved the Histopathology of Skeletal Muscle in Dystrophic Mice

[1]Aiping Lu; [2] Qing Yang; [1]Minakshi Poddar; [1]Bing Wang; [3]Denis C. Guttridge; [4]Paul D. Robbins; [1]+ Johnny Huard
[1]+Stem Cell Research Center and Department of Orthopaedic Surgery, University of Pittsburgh, Pittsburgh, PA
[2]Department of Orthopaedic Surgery, Tongji Hospital, Huazhong University of Science and Technology, Wuhan, China
[3]Department of Molecular Virology, Immunology and Medical Genetics, Ohio State University, Columbus, OH
[4]Department of Microbiogy and Molecular Genetics. University of Pittsburgh, Pittsburgh, PA
jhuard@pitt.edu

INTRODUCTION

Duchenne muscular dystrophy (DMD) is a deadly genetic disease mainly characterized by progressive weakening of the skeletal, cardiac and diaphragmatic muscles. It is critical to find a successful therapy that will improve the histopathology of the muscles of DMD patients and restore their normal function. Recent studies have demonstrated that blocking p65, a subunit of NF-κB, enhances muscle regeneration in injured and diseased skeletal muscle [1, 2], which suggests that the NF-kB signaling pathway is a contributing factor to the dystrophic pathology in DMD patients. Previously we demonstrated that muscle derived stem cells (MDSCs) isolated from the skeletal muscles of heterozygote P65 knock-out (*P65*$^{+/-}$) mice showed better muscle regeneration *in vitro* and *in vivo* compared to the MDSCs isolated from wild-type (WT) mice. We also demonstrated that the transplantation of P65$^{+/-}$ MDSCs could reduce inflammation. Based on these results we performed a set of experiments to determine if these P65$^{+/-}$ MDSCs could alleviate the pathology associated with DMD more efficiently than wild-type MDSCs. When we injected p65$^{+/-}$ MDSCs intraperitoneally into dystrophin/utrophin deficient (dys-/-:utro-/-, dKO) mice, a reliable mouse model of DMD, we found that the histopathology of various skeletal muscles improved and observed a reduction in inflammation, necrosis and pathological muscle regeneration.

MATERIALS AND METHODS

Cell Isolation: MDSCs were isolated from 5 month old P65$^{+/-}$ and WT mice as previously described via a modified preplate technique [3]. The cell suspensions from both P65$^{+/-}$ and WT muscle were plated on collagen coated flasks and cultured in proliferation medium (DMEM supplemented with 10% fetal bovine serum, 10% horse serum, 0.5% chicken embryo extract and 1% Penicillin-streptomycin) until the cell number was sufficient for injection.

***Intraperitoneal injection* (IP):** A total of 5-9 x10^5 viable cells were suspended in 50 µl of PBS and injected IP into 5-7 days old of dKO mice. Four to six weeks after transplantation, the mice were sacrificed and their muscles were harvested and flash frozen in liquid nitrogen-cooled 2-methylbutane. 10µm serial cryosections were prepared from the frozen muscle.

Immunohistocytochemistry

Cryosections were fixed with 5% formalin, blocked with 5% Donkey serum, and then incubated with an antibody against mouse IgG (Biotinlated) to determine the extent of muscle fiber necrosis. An antibody against embryonic muscle heavy chain (E-MyHC) was used to evaluate myogenic regeneration and an antibody against F4/80 (macrophage marker) was used to analyze the extent of inflammation in the muscle tissues. Streptavidin Cy3 conjugate and Alexafluor 488 conjugated anti-mouse IgG were used as secondary antibodies. H&E staining was performed to assess myofiber morphology and fibrosis.

RESULTS

Transplantation of P65+/- MDSCs improved muscle histology

H&E showed histology improvement in various skeletal muscles including the gastrocnemius, diaphragm, thigh and tibialis anterior muscles. We observed many centrally nucleated muscle fibers (new regenerated fibers) and decreased fibrosis in the p65$^{+/-}$ MDSC injection group (**Figure 1,** thigh muscle**)**.

Transplantation of P65+/- MDSCs reduced muscle necrosis

Mouse IgG staining showed that there were less necrotic muscle fibers in the mice injected with p65$^{+/-}$ MDSCs compared to the un-treated muscle **(Figure2)**

Transplantation of P65$^{+/-}$ MDSCs reduced inflammation and pathological muscle regeneration

Less inflammation and E-MyHC positive myofibers were found in the muscles of mice injected with p65$^{+/-}$ MDSCs compared to non-treated muscle **(Figure3).**

Figure1

DKO untreated muscle **DKO muscle treated with MDSCs**

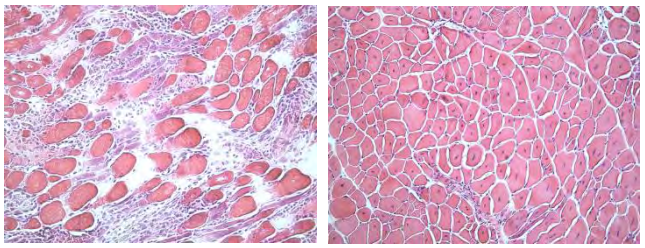

Figure2

DKO untreated muscle **DKO muscle treated with MDSCs**

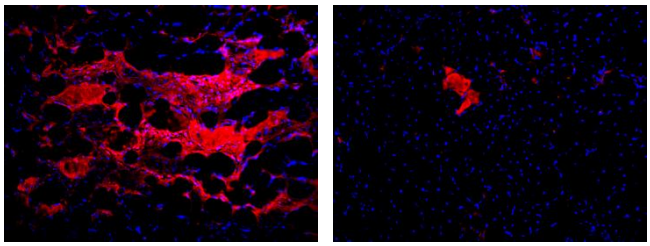

Figure3

DKO muscle nontreated **DKO muscle treated with MDSCs**

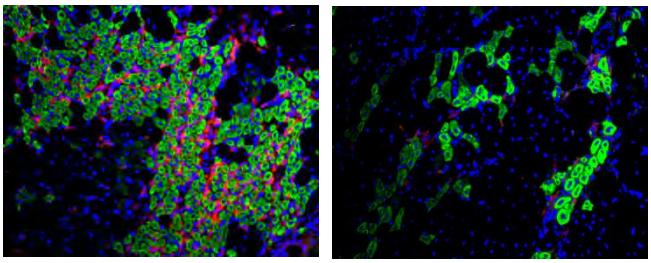

DISCUSSION

In this study we used MDSCs isolated from p65+/- mice to treat dystrophin-/-utrophin-/- mice. The up-regulation of the NF-κB pathway in these mice is associated with chronic inflammation which results in pathologies such as muscle fibrosis, necrosis, and muscle wasting. Our findings indicated that blocking p65, a subunit of NF-κB, can decrease macrophage infiltration, fibrosis formation, necrosis, and diminishes pathologic regeneration in 4 to 6 week dKO mice. We also attempted to inject the WT MDSCs isolated from normal animals; however, the results did not show an improvement in the histopathology of the mice. These results suggest that reducing the activity of the IKK/NF-κB pathway is a potential therapeutic target for the treatment of DMD. These are only preliminary data; however they are very exciting and we are planning to test additional animals in order to further confirm these results.

REFERENCES:

[1] Thaloor, D, et al Am. J.Physiol 1999; 277:C320–C329. [2] Acharyya S et al, J. Clin. Invest 2007 ; 117 :889-901. [3] Gharaibeh, et al. Nat Protoc. 2008; 3:1501-9

Immunomodulatory properties of muscle-derived stem cells associated with reduced NF-κB/p65 signaling

[1]Proto, J.; [1]Lu, A.; [2]Robbins, P.D.; [1]+Huard, J.
[1]+ Stem Cell Research Center, Children's Hospital of Pittsburgh, and Department of Orthopedic Surgery;
[2]Departments of Microbiology and Molecular Genetics, University of Pittsburgh School of Medicine, Pittsburgh, PA
jhuard@pitt.edu

INTRODUCTION

The nuclear factor kappa B (NF-kB) signal pathway has been implicated in both the normal and disease states of many different tissues. In skeletal muscle, for example, constitutive activation of inhibitor of kappa B kinase (IKKβ), a potent activator of NF-kB, leads to muscle wasting[1]. Inversely, muscle specific deletion of IKKβ in a murine model of muscular dystrophy improves dystrophic pathology and is accompanied by an increase in the number of cells fitting a muscle progenitor marker profile ($CD34^+/Sca1^-$), suggesting that NF-kB has a direct effect on muscle stem cells[2]. The NF-kB protein family includes five subunits, two of which, a p65-p50 heterodimer, are thought to play a role in blocking early myogenesis[3]. In this study, we examined the role of NF-kB signaling in the regenerative phenotype of muscle-derived stem cells (MDSCs) isolated from the gastrocnemius of p65 deficient mice (heterozygous, $p65^{+/-}$) and wild type littermates ($p65^{+/+}$). We previously found that $p65^{+/-}$ MDSCs have enhanced cell proliferation, survival under oxidative stress, differentiation, and muscle regeneration capacity. Furthermore, we have found that $p65^{+/-}$ engraftments in wild type skeletal muscle are associated with reduced inflammation and fiber necrosis compared to $p65^{+/+}$ MDSC engraftments. *In vitro* and *in vivo* experiments suggest that reduction of p65 signaling enhances the regenerative phenotype of MDSCs, suggesting this pathway as a candidate target to improve stem cell-based therapies for muscle disease and injury.

MATERIALS AND METHOD

Cell Isolation: MDSCs were isolated from five month old (n=3) $p65^{+/+}$ or $p65^{+/-}$ mice via a preplate technique [4]. A population of slowly adhering cells was obtained and expanded in DMEM containing 10% fetal bovine serum (FBS), 10% horse serum, 1% penicillin-streptomycin, and 0.5% chick embryo extract. Cells were used between passages 15 and 30.

In vivo regeneration assay: Muscle injury was induced in C57Bl/6J mice by cardiotoxin injected into gastrocnemius. One day later, MDSCs were injected into the injured muscles. Six days following transplantation, mice were sacrificed and injected muscles were harvested and snap-frozen. Serial cryosections were prepared and immunohistochemistry was performed to assess inflammation (CD14) and necrosis (IgG). The number of CD14 (+) cells was counted to assess infiltration of macrophages/monocytes. Necrosis was determined by mouse IgG staining and quantified by assessing the percentage of positively stained area.

In vitro Inflammation Model: MDSCs were grown for 24 hours in proliferation medium, after which the medium was collected and sterile filtered. RAW264.7 cells, immortal murine macrophage-like cells, were activated by exposure to 100 ng/mL LPS in either $p65^{+/+}$-, $p65^{+/-}$-, or muscle-derived fibroblast conditioned medium for 24 hours.

***Gene Expression Analysis*:** Cells were washed and RNA collected by Trizol extraction. Total RNA was reverse transcribed with Superscript III reverse transcriptase (Invitrogen) according to manufacturer's protocols. The PCR reaction was carried out with Taq Polymerase (Promega), according to manufacturer's protocols. PCR products were analyzed by electrophoresis on a 1.5% agarose gel

RESULTS

Wild type mice were injected with either $p65^{+/+}$ (Fig 1A) or $p65^{+/-}$ (Fig 1B) MDSCs in the gastrocnemius muscle and sacrificed six days later. Tissues were cryosectioned and immunostained with antibodies against CD14 to identify a monocyte/macrophage infiltrate, indicating inflammation, as well as with antibodies against mouse immunoglobulin G, a marker of necrosis. Injections of $p65^{+/-}$ cells were associated with a decrease in both necrosis and inflammation (Fig 1B-D), compared to $p65^{+/+}$ injections (Fig1A, C-D).

Figure 1.

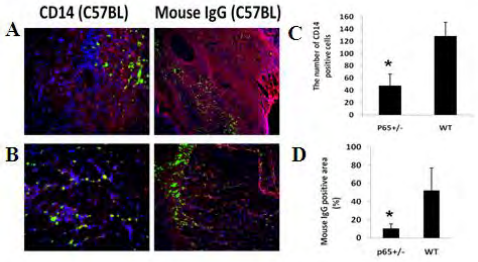

To investigate anti-inflammatory properties of MDSCs, we utilized an *in vitro* inflammation model in which RAW264.7 cells, immortal murine macrophage-like cells, are activated by LPS exposure. We found that RAW264.7 cells exposed to LPS in $p65^{+/-}$ CM expressed less IL-1 compared to controls, suggesting that p65+/- MDSCs secrete immunomodulatory factors that hinder pro-inflammatory macrophage activation.

Figure 2.

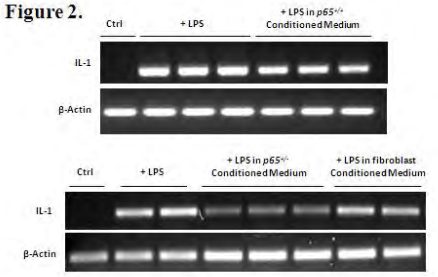

DISCUSSION

The data presented here provides evidence supporting that NF-kB inhibition stimulates MDSC-mediated muscle regeneration through multiple mechanisms, including through the expression of anti-inflammatory factors that attenuate inflammation and necrosis. These experiments identify the NF-κB signaling pathway as a potential therapeutic target to enhance muscle regeneration following injury or disease. Future directions for this project include investigating modulation of the IKK/NF-kB pathway as a means to rejuvenate the phenotype of aged muscle stem and progenitor cells. Clinical research should be conducted to test the efficacy of p65 inhibition therapy in patients suffering from muscle disorders.

REFERENCES

[1]Cai, D., et al. Cell 2004, 119:285-298. [2]Acharyya, S., et al., J Clin Invest 2007, 117:889-901. [3]Bakkar, N., et al. JCB 2008, 180(25): 787-802. [4] Gharaibeh, et al. Nat Protoc. 2008; 3:1501-9